Exhumation of the Inyo Mountains, California: Implications for the timing of extension along the western boundary of the Basin and Range Province and distribution of dextral fault slip rates across the eastern California shear zone

Jeffrey Lee,[1] Daniel F. Stockli,[2] Lewis A. Owen,[3] Robert C. Finkel,[4] and Roman Kislitsyn[2]

Received 28 March 2008; revised 22 October 2008; accepted 13 November 2008; published 23 January 2009.

[1] New geologic mapping, tectonic geomorphologic, ^{10}Be terrestrial cosmogenic nuclide, and (U-Th)/He zircon and apatite thermochronometric data provide the first numerical constraints on late Cretaceous to late Quaternary exhumation of the Inyo Mountains and vertical slip and horizontal extension rates across the eastern Inyo fault zone, California. The east-dipping eastern Inyo fault zone bounds the eastern flank of the Inyo Mountains, a prominent geomorphic feature within the western Basin and Range Province and eastern California shear zone. (U-Th)/He zircon and apatite thermochronometry yield age patterns across the range that are interpreted as indicating: (1) two episodes of moderate to rapid exhumation associated with Laramide deformation during the late Cretaceous/early Tertiary; (2) development of a slowly eroding surface during a prolonged period from early Eocene to middle Miocene; (3) rapid cooling, exhumation, and initiation of normal slip along the eastern Inyo fault zone, accommodated by westward tilting of the Inyo Mountains block, at 15.6 Ma; and (4) rapid cooling, exhumation, and renewed normal slip along the eastern Inyo fault zone at 2.8 Ma. Fault slip continues today as indicated by fault scarps that cut late Pleistocene alluvial fan surfaces. The second episode of normal slip at 2.8 Ma also signals onset of dextral slip along the Hunter Mountain fault, yielding a Pliocene dextral slip rate of 3.3 ± 1.0 mm/a, where a is years. Summing this dextral slip rate with estimated dextral slip rates along the Owens Valley, Death Valley, and Stateline faults yields a net geologic dextral slip rate across the eastern California shear zone of 9.3 + 2.2/−1.4 to 9.8 + 1.4/−1.0 mm/a.

Citation: Lee, J., D. F. Stockli, L. A. Owen, R. C. Finkel, and R. Kislitsyn (2009), Exhumation of the Inyo Mountains, California: Implications for the timing of extension along the western boundary of the Basin and Range Province and distribution of dextral fault slip rates across the eastern California shear zone, *Tectonics*, *28*, TC1001, doi:10.1029/2008TC002295.

1. Introduction

[2] Overlap of E-W extension along the western margin of the Basin and Range Province by NW dextral shear characteristic of the eastern California shear zone (ECSZ) defines a broad, active, complex intracontinental deformation zone (Figure 1). The interaction between continental extension and dextral shear within this region of the U.S. Cordillera makes it one of the world's best places to examine the relative contributions of plate boundary forces and internal driving forces to intracontinental deformation kinematics. Data from GPS, topographic, geoid, and Quaternary fault slip studies have been used to hypothesize that NW dextral shear and E–W extension within the ECSZ resulted from translation of the Sierra Nevada both parallel and perpendicular to the Pacific-North American plate boundary in consequence of plate tractions and gravitational potential energy, respectively [e.g., *Flesch et al.*, 2000; *Bennett et al.*, 2003; *Hammond and Thatcher*, 2004]. Petrological, geochemical, and geophysical investigations centered on Sierra Nevada lithospheric structure and young deformation along the western boundary of the Basin and Range Province led *Jones et al.* [2004, and references therein] to suggest that removal of lithosphere beneath the Sierra Nevada at ~3.5 Ma initiated uplift and onset of extension within ~50 km of the east side of the range. *Jones et al.* [2004] further suggested that initiation of Pliocene extension along the western margin of the Basin and Range Province was driven by the increase in gravitational potential energy as a consequence of Sierra Nevada uplift and postulated that a combination of locally derived internal forces (gravitational potential energy) and plate boundary forces drive fault kinematics along the western boundary of the ECSZ and Basin and Range Province.

[1]Department of Geological Sciences, Central Washington University, Ellensburg, Washington, USA.
[2]Department of Geology, University of Kansas, Lawrence, Kansas, USA.
[3]Department of Geology, University of Cincinnati, Cincinnati, Ohio, USA.
[4]Center for Accelerator Mass Spectrometry, Lawrence Livermore National Laboratory, Livermore, California, USA.

0278-7407/09/2008TC002295$12.00

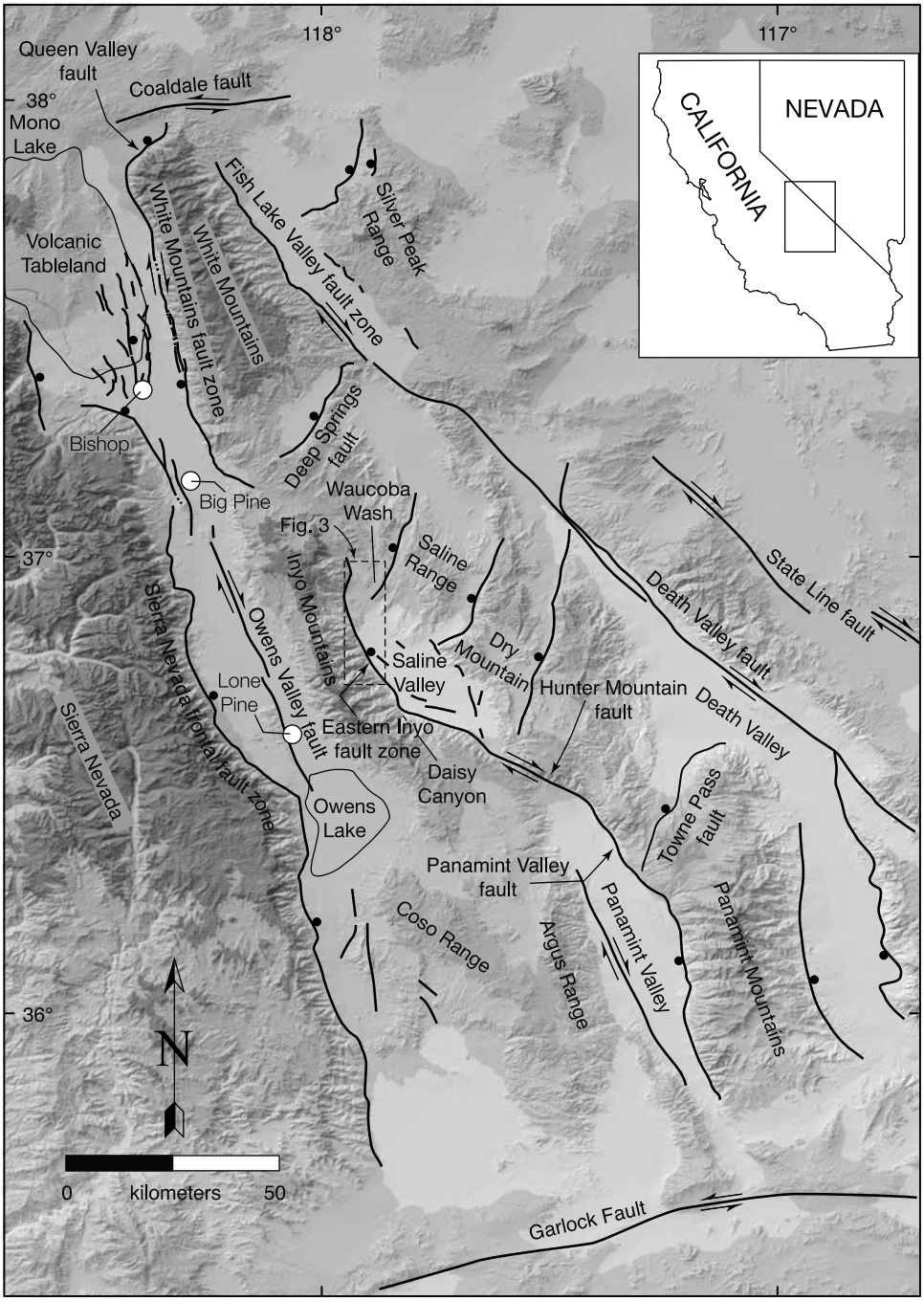

Figure 1. Shaded relief map of a part of the eastern California shear zone and western Basin and Range Province, showing major Quaternary faults. Solid circles are on the hanging wall of normal faults; arrows indicate relative motion across strike-slip faults. Dashed box outlines location of Figure 3.

[3] Dextral shear, across an ~100–200 km wide zone north of the Garlock fault that defines this segment of the ECSZ, is accommodated along four major NNW-striking strike-slip fault zones (the Stateline, the Death Valley-Fish Lake Valley, Hunter Mountain-Panamint Valley, and Owens Valley-White Mountains fault zones) and a series of connecting NE-striking normal faults such as the Towne Pass, Deep Springs, and Queen Valley faults (Figure 1). Geologic and geodetic data indicate that the ECSZ is an important component of the Pacific-North American plate boundary zone [e.g., *Dokka and Travis*, 1990; *Gan et al.*, 2000; *Bennett et al.*, 2003; *Frankel et al.*, 2007]. Results from recent GPS (Global Positioning System) measurements indicate a right lateral shear rate of 9.3–13.9 mm/a, where a is years, across the zone, accounting for ~20–25% of the total relative plate motion [e.g., *Gan et al.*, 2000; *Bennett et*

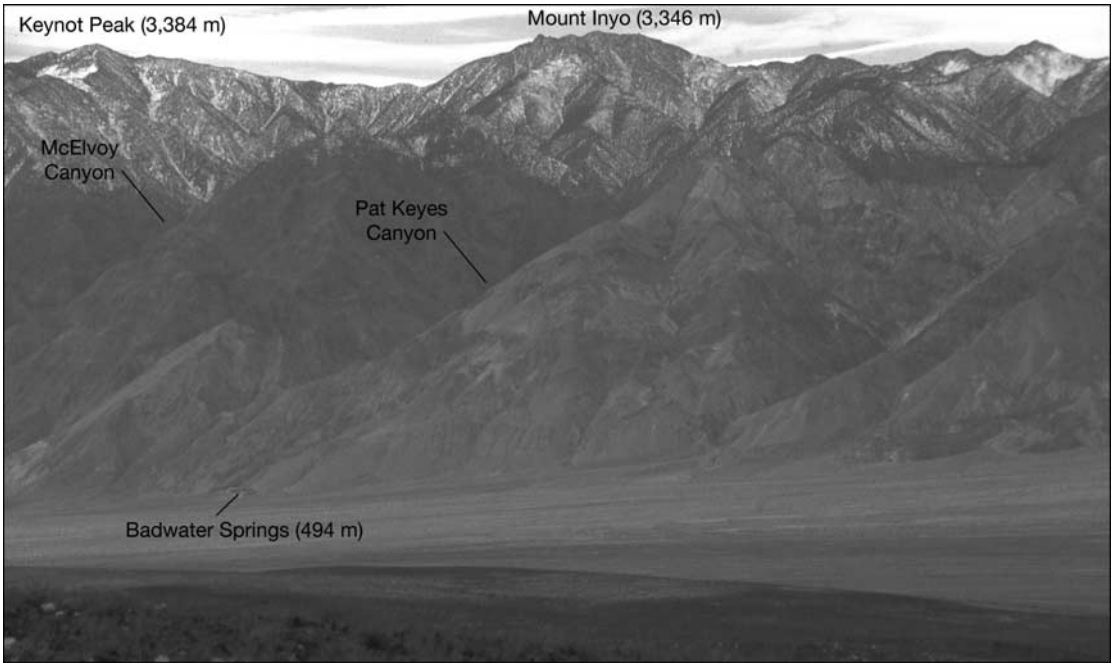

Figure 2. View southwest at the central part of the eastern flank of the Inyo Mountains. The EIFZ is exposed at the base of the mountains; Badwater Springs is located along the trace of the fault. Height of the footwall escarpment above the valley floor is a maximum of ~3.0 km at McElvoy Canyon. Zircon and apatite (U-Th)/He sample transect is located along the ridgeline north of Pat Keyes Canyon.

al., 2003]. A sum of geologic slip rates across this zone yields net dextral slip rates of 8.5–10 mm/a [*Frankel et al.*, 2007], the same, within error, to the geodetic rates. The similarity between geodetic and geologic slip rates in this part of the ECSZ suggests that the transient strain accumulation observed in the ECSZ south of the Garlock fault does not continue to the north [cf. *Rockwell et al.*, 2000; *Peltzer et al.*, 2001; *Oskin and Iriondo*, 2004; *Frankel et al.*, 2007; *Oskin et al.*, 2007].

[4] The geometry, kinematics, magnitude, and timing of fault slip throughout this region are critical for testing these geodynamic hypotheses and for comparing geodetic slip rates to geologic slip rates. The Inyo Mountains is one of the most prominent geomorphic features in this region. This mountain range is ~95 km long and 20–25 km wide with a maximum relief of ~3000 m, rising to its highest point at 3390 m above sea level (Figure 2). Little is known, however, about the tectonic and geomorphic development of the range. The Inyo Mountains are bounded along its east flank by an active, east-dipping normal fault system, the eastern Inyo fault zone (EIFZ). The EIFZ can be traced for ~40 km from Daisy Canyon in the south to Waucoba Wash to the north (Figures 1 and 3). Saline Valley, with a maximum depth to basement of 4.0–4.5 km [*Blakely and Ponce*, 2001], is a pull-apart basin exposed in its hanging wall (Figures 1 and 3).

[5] The Inyo Mountains are located within a unique kinematic configuration in this part of the Basin and Range Province and ECSZ. These mountains are the southern continuation of the White Mountains, an east-tilted normal fault block [*Stockli et al.*, 2003], and are parallel to and lie east of the Sierra Nevada, a west-tilted normal fault block. The Inyo Mountains form the northern termination of the Hunter Mountain fault, a NW-striking dextral fault that connects the relatively shallow Panamint Valley (<1 km to basement at the northern end [*Blakely and Ponce*, 2001]) and much deeper Saline Valley pull-apart basins [e.g., *Burchfiel et al.*, 1987; *Oswald and Wesnousky*, 2002] (Figure 1).

[6] In this paper, we describe the first zircon and apatite (U-Th)/He thermochronologic results from across the Inyo Mountains that characterize its low-temperature cooling, exhumation, and tilting histories and geologic mapping and terrestrial cosmogenic radionuclide (TCN) ages for alluvial fans along the eastern piedmont of the Inyo Mountains that document its young faulting history. From these data, we infer late Cretaceous/early Tertiary exhumation associated with Laramide deformation followed by a protracted period of slow erosion, and middle Miocene to late Pleistocene fault slip rates along EIFZ that bear on the development of the Inyo Mountains as a major topographic feature and its tectonic role in the development of this part of the Basin and Range Province and ECSZ.

2. Geologic Setting

[7] The Inyo Mountains expose several Mesozoic granitic plutons, associated with emplacement of the Sierra Nevada batholith [e.g., *Bateman et al.*, 1963; *Ross*, 1969; *Sylvester et al.*, 1978; *Bateman*, 1992; *Dunne and Walker*,

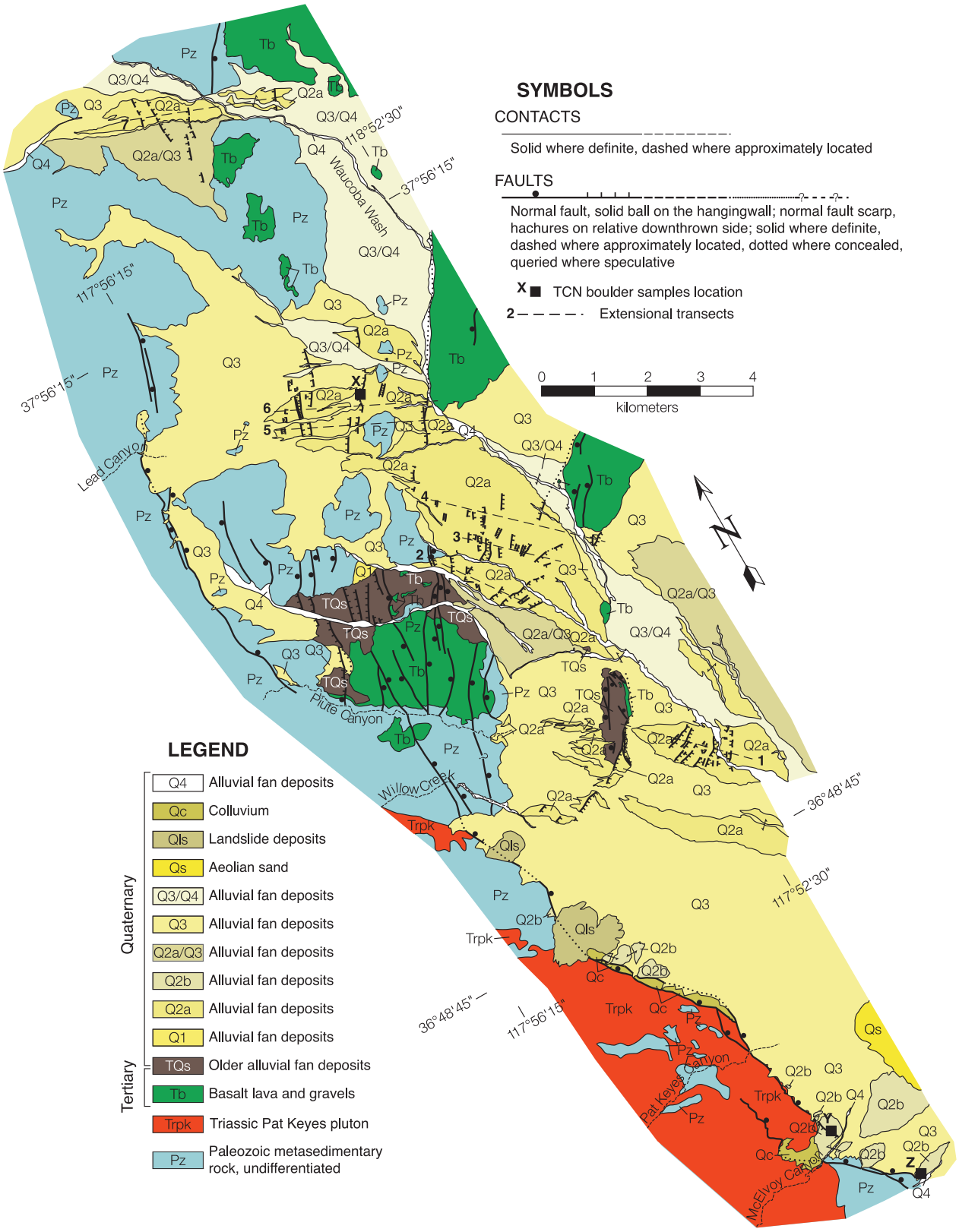

Figure 3. Geologic map along the eastern Inyo fault zone showing pre-Tertiary rocks, Tertiary volcanic rocks, Quaternary sedimentary deposits and alluvial fan surfaces, and Quaternary faults. Location of cosmogenic radionuclide samples and extensional transects shown. Location of geologic map is shown in Figure 1. Bedrock geology from *Ross* [1967].

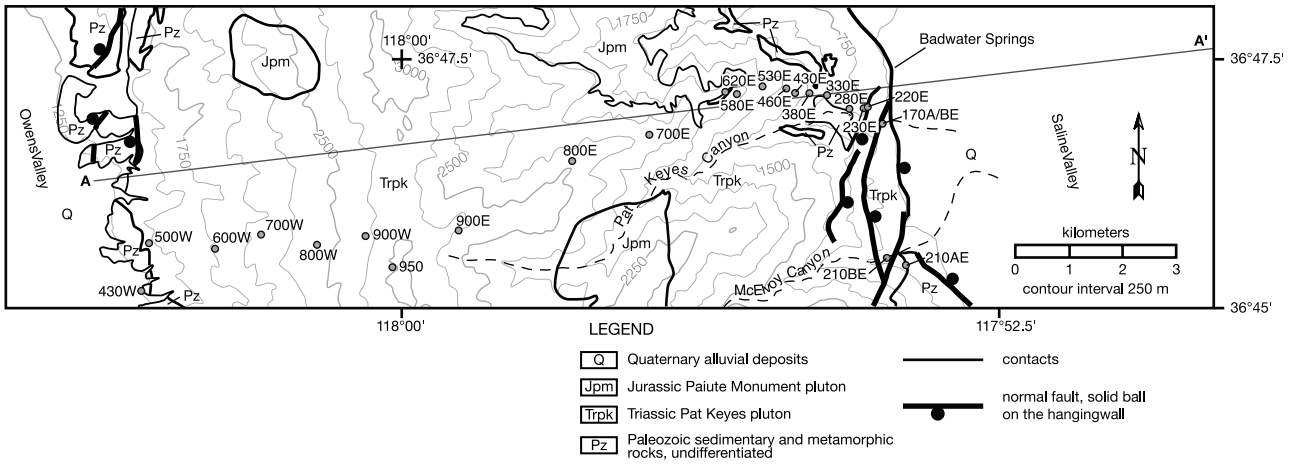

Figure 4. Simplified geologic map across the central Inyo Mountains showing location of (U-Th)/He thermochronometric samples. Geology from *Ross* [1967].

2004], which intrude into sedimentary rocks including Precambrian through Paleozoic miogeocline strata [e.g., *Ross*, 1967; *Stevens et al.*, 1997] and Mesozoic marine and nonmarine volcanic and epiclastic strata [*Ross*, 1967; *Dunne et al.*, 1998] (Figures 3 and 4). The largest of the plutons is the Pay Keyes pluton, a heterogeneous plutonic body well exposed throughout the central part of the mountain range. The composition of the Pat Keyes pluton ranges from quartz monzonite to monzonite-granodiorite to a variety of mafic intrusive rocks [*Ross*, 1969]. Zircon from the Pat Keyes pluton yielded a Pb-α age of 210 ± 20 Ma [*Ross*, 1965], whereas a whole rock, biotite, and muscovite Rb/Sr isochron yielded an age of 183 Ma [*Dunne*, 1971]. In the southwestern Inyo Mountains, Paleozoic and Mesozoic metasedimentary rocks were complexly folded and faulted during the Permian, Jurassic, and Cretaceous [e.g., *Stone et al.*, 2004; *Dunne and Walker*, 2004].

[8] In the southeastern Inyo Mountains, *Conrad* [1993] mapped a middle to late Miocene sedimentary basin that was deposited over, but not cut by, the southern extension of the EIFZ. Alluvial fan and gravel deposits that make up this basin were sourced from the uplifted footwall Inyo Mountains to the west. Exposed near the base of these gravel and fan deposits is a reworked 13.62 ± 0.52 Ma ($^{40}Ar/^{39}Ar$ age) tephra [*Conrad*, 1993], indicating that most of these deposits are younger than middle Miocene. These basin deposits do not contain basalt clasts, suggesting they are older than the ~4–6 Ma basalt lavas in the region [*Larsen*, 1979; *Casteel*, 2005].

[9] Late Cenozoic faults, including the EIFZ, a dominantly normal slip fault, and the Hunter Mountain fault zone, a dominantly dextral fault, bound the east flank of the Inyo Mountains. Late Cenozoic faults are not exposed along the western flank of the Inyo Mountains except for the oblique slip southern Inyo Mountains fault along the SW Inyo Mountains [*Bacon et al.*, 2005; *Casteel*, 2005]. Nevertheless, a steep, linear gravity gradient along the western front of the Inyo Mountains has been interpreted as a continuous bedrock fault scarp buried beneath thick alluvial fan deposits [*Pakiser et al.*, 1964].

3. Methods of Study

[10] Geologic mapping along the EIFZ and across the northern part of Saline Valley was completed on a 1:24,000 scale aerial photographs and 1:12,000 scale digital orthophotoquadrangles. We used (U-Th)/He thermochronometry on zircon and apatite, a powerful approach to documenting the low- to moderate-temperature cooling and exhumation history of the Inyo Mountains and to dating normal fault motion [e.g., *Ehlers*, 2005; *Stockli*, 2005]. This approach is limited only by whether exhumation was of sufficient magnitude to expose rocks that resided at temperatures above the blocking temperature of the minerals in question. (U-Th)/He dating of zircon and apatite is an effective and well-established low- to moderate-temperature thermochronometric technique [e.g., *Zeitler et al.*, 1987; *Wolf et al.*, 1996, 1998; *House et al.*, 1997, 1999; *Farley*, 2000; *Reiners et al.*, 2000; *Reiners*, 2005; *Stockli*, 2005]. Zircon and apatite (U-Th)/He thermochronometry is characterized by closure temperatures of ~185°C and ~70°C, respectively, and partial retention zones between ~190–130°C and ~80–40°C, respectively [*Wolf et al.*, 1996, 1998; *House et al.*, 1999; *Stockli et al.*, 2000; *Tagami et al.*, 2003; *Stockli*, 2005; *Wolfe et al.*, 2007]. These allow characterization of exhumation histories at relatively shallow crustal levels. TCN dating of alluvial fan boulders was used to define the age of abandonment of alluvial surfaces exposed along the east flank of the Inyo Mountains. Zircon and apatite (U-Th)/He and TCN sample processing and analytical procedures are described in the Auxiliary Material.[1]

[11] Global Positioning System (GPS) precise point kinematic (PPK) surveys using dual frequencies L1/L2 GPS receivers were used to measure the oblique slip offset

[1] Auxiliary materials are available in the HTML. doi:10.1029/2008TC002295.

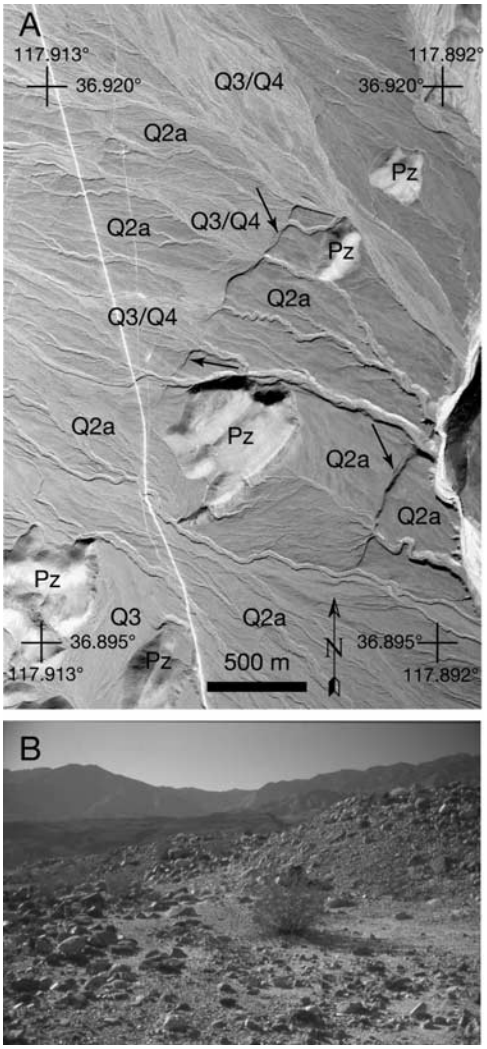

Figure 5. Characteristics of deformed alluvial fan surfaces. (a) Aerial photograph showing surface character of Quaternary alluvial fan surfaces and normal fault scarps (indicated by arrows) in the southern Waucoba Wash. Pz, undifferentiated Paleozoic bedrock. (b) View to west of a SE-facing fault scarp developed within a Q2a alluvial fan surface. Surface offset of ~2.6 m across the scarp. Inyo Mountains are in the background.

of debris flow levees across fault scarps and a tape measure and compass were used to measure the vertical offset of alluvial fan surfaces across normal fault scarps. Maximum vertical offsets of alluvial surfaces were calculated geometrically using the middle of the fault scarp [after *Hanks et al.*, 1984]. Errors associated with lateral offset measurements include GPS survey points ($\leq$10 cm) and visually defining the location of the geomorphic feature in the field (0.5–1.0 m); we report the latter error because it is the larger of the two and hence provides a conservative estimate of slip rates. Errors associated with the vertical offset measurements include far field slope and scarp angle measurements (typically 1–3°) and fault scarp downdip length measurement (0.2–0.3 m); these errors are incorporated into the calculation of the vertical offset.

4. Late Cenozoic Rock Units and Ages

[12] The EIFZ, from Daisy Canyon northward, cuts and offsets bedrock in the Inyo Mountains, Pliocene basalt and andesite lava flows, and granite- and metamorphic derived Quaternary coarse- to fine-grained alluvial fan and debris flow deposits (Figures 1 and 3).

[13] Unit Tb, composed of Pliocene basalt and andesite lavas, locally interbedded with subangular to subrounded gravels at its base, underlie the Saline Range and small bedrock mounds in northern Saline Valley [*Ross*, 1970; *Sternlof*, 1988]. Whole rock samples from these typically porphyritic plagioclase ± clinopyroxene ± olivine-bearing lavas yield K/Ar ages that range from 1.4 ± 0.1 Ma to 3.7 ± 0.7 Ma [*Ross*, 1970; *Larsen*, 1979; *Elliot et al.*, 1984; *Sternlof*, 1988].

[14] Unit Tqs overlies unit Tb and comprise fanglomerates that are composed of massive, indurated, poorly sorted, angular sand to boulder-sized clasts, which have been derived from older units.

[15] Along the eastern piedmont of the Inyo Mountains and across the northern part of Saline Valley, four distinct Quaternary alluvial fan surfaces were mapped on the basis of surface morphology, including degree of dissection, inset geometry, height above present-day stream grade, surface texture, and tone or color on aerial photographs.

[16] A small remnant of the oldest alluvial fan surface, Q1, is exposed in the central part of the map area 15–20 m above present-day channels. This surface possesses a well-developed desert pavement, rounded and dissected morphology, and appears light colored in aerial photographs.

[17] The degree of surface dissection and morphology allows Q2 surfaces to be subdivided into two mappable units. In Waucoba Wash, at the northern end of Saline Valley, the older Q2 surfaces, Q2a, are generally weakly dissected smooth surfaces with widely (>100 m) spaced, up to ~10 m deep channels, and moderately to weakly developed desert pavement; these surfaces appear dark in aerial photographs (Figure 5). Three quartzite boulders collected from a Q2a surface yield a mean ^{10}Be TCN model surface age of 44.3 ± 12.1 ka (1 standard deviation) (sample location X in Figure 3, see also Table 1). The younger Q2b surfaces are generally exposed at the apex of alluvial fan aprons along the eastern Inyo Mountains range front. Alluvial fan deposits underlying these triangular-shaped surfaces are sourced from east-draining canyons; cross-fan profiles are convex up. These surfaces are debris flow dominated with channels up to 5 m deep. On aerial photographs, these surfaces appear dark. Six granite boulders were dated from a Q2b alluvial fan surface at the mouth of McElvoy Canyon and four from a similar surface ~2 km to the southeast (sample locations Y and Z, respectively, in Figure 3, see also Table 1). Four boulder samples from McElvoy Canyon yield a mean ^{10}Be TCN model surface age of 18.3 ± 4.4 ka, whereas two boulder samples yield ages of 91.2 ± 10.2 and 35.5 ± 3.4 ka, $\geq$70% older than the

Table 1. Summary of Terrestrial Cosmogenic Nuclide Sample Parameters, Analytical Data, and Calculated ^{10}Be Model Ages for Quartzite Boulder Samples Collected From Three Different Alluvial Fan Surfaces in Saline Valley, California

Sample Number[a]	Latitude (N)[b]	Longitude (W)[b]	Altitude (m)	Shielding Factor	Boulder Size (Height/ Intermediate Axis/Long Axis) (cm)	Quartz Mass (g)	Concentration of ^{9}Be Carrier (mg/g)	Mass of ^{9}Be Carrier (g)	^{9}Be/^{10}Be (10^{-15})[c]	^{10}Be Measured (atoms g^{-1})	Production Rate (Spallation) (atoms/g/a)	Production Rate (Muons) (atoms/g/a)	^{10}Be Exposure age (ka)[d]	Internal Uncertainty (years)[e]	External Uncertainty (ka)[e]
Waucoba Wash, Fan Surface Q2a															
SV20	36°54.651	117°54.100	1057	1.0000	20/70/120	26.5786	26.5786	0.404	434.67 ± 14.65	411348 ± 14530	9.99	0.278	43.4	1669	4.4
SV21	36°54.538	117°54.167	1056	1.0000	35/50/70	26.9428	1.4932	0.404	233.25 ± 6.44	315994 ± 8718	9.98	0.278	32.7	963	3.2
SV23	36°54.432	117°54.296	1057	1.0000	40/80/100	24.6696	24.6696	0.404	524.02 ± 12.83	525033 ± 13646	9.98	0.278	56.8	1650	5.7
													Mean age ±1 standard deviation	44.3	12.1
McElvoy Canyon, Fan Surface Q2b															
SV9[f]	36°45.817	117°53.577	512	0.9768	40/60/100	10.806	10.806	0.404	216.54 ± 6.09	510794 ± 17977	6.37	0.233	91.2	3841	10.2
SV10[f]	36°45.809	117°53.592	513	0.9753	60/70/140	19.0865	1.0452	0.389	170.23 ± 4.23	219486 ± 5445	6.37	0.233	35.5	943	3.4
SV11	36°45.814	117°53.587	512	0.9733	25/60/75	21.84	1.07	0.389	113.13 ± 4.45	130381 ± 5134	6.35	0.233	20.6	843	2.0
SV12	36°45.692	117°53.479	538	0.9788	70/70/120	21.752	1.007	0.389	71.05 ± 3.33	77425 ± 3633	6.52	0.235	11.7	562	11.8
SV13	36°45.688	117°53.492	543	0.9797	60/120/120	13.6048	1.0532	0.389	71.48 ± 4.27	130234 ± 7776	6.55	0.235	19.9	1235	21.8
SV14	36°45.691	117°53.481	537	0.9791	20/60/110	15.766	15.766	0.404	85.80 ± 3.69	135218 ± 9263	6.52	0.235	20.8	1484	23.9
													Mean age ±1 standard deviation	18.3	4.4
South of McElvoy Canyon, Fan Surface Q2b															
SV15	36°44.940	117°52.793	442	0.9750	60/100/160	20.7717	1.0479	0.404	60.36 ± 4.00	89052 ± 8967	6.01	0.227	14.7	1519	2.0
SV16	36°44.938	117°52.803	462	0.9743	25/50/80	20.2674	0.9731	0.404	74.65 ± 3.79	148561 ± 7533	6.11	0.229	24.5	1305	2.6
SV17	36°44.937	117°52.791	459	0.9741	20/65/40	15.0935	0.9715	0.404	40.18 ± 3.36	85348 ± 12068	6.09	0.229	13.9	2013	2.4
SV18[f]	36°44.925	117°52.821	469	1.0000	70/80/110	18.2053	0.9033	0.404	229.44 ± 5.88	278281 ± 7131	6.30	0.230	46.4	1301	4.6
													Mean age ±1 standard deviation	17.7	5.9

[a]All boulder samples are quartzite.
[b]World Geodetic System 84 datum.
[c]The ^{9}Be/^{10}Be ratios were corrected for background and blanks (SV-blank1 and SVBLK with ^{9}Be/^{10}Be ratios of $25.16 \pm 1.66 \times 10^{-15}$ and $26.77 \pm 1.44 \times 10^{-15}$, respectively).
[d]Ages were calculated using a density of 2.7 g/cm^3 and a sample thickness of 5 cm.
[e]Internal uncertainty considers only the analytical uncertainty (reported to 1σ as per convention), while external uncertainty incorporates production rate uncertainties.
[f]Sample age not used in calculating mean age.

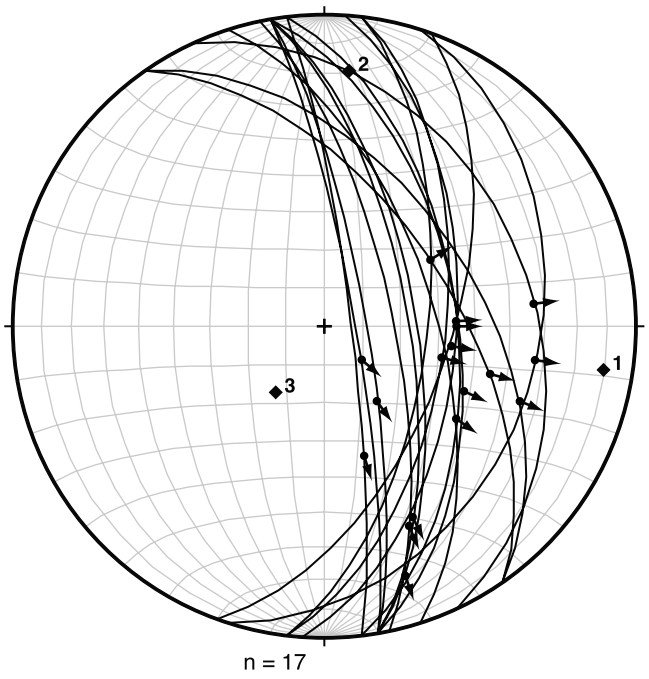

Figure 6. Lower hemisphere equal area stereonet of fault planes (great circles), fault striations (arrows), and kinematic axes (solid diamonds) for fault/striation data pairs along the eastern Inyo fault zone. Data from *O'Malley* [1980] and this study. 1, extension axis; 2, intermediate axis; 3, shortening axis.

other four samples. Three boulder samples collected from a similar surface to the southeast yield a mean ^{10}Be model surface age of 17.7 ± 5.9 ka. One boulder sample from this surface yields an age of 46.4 ± 4.6, ≥89% ka older than the other three samples. We suggest that inheritance likely explains these older boulder ages.

[18] The really dominant alluvial fan surface, both along the range front and across northern Saline Valley, is Q3 (Figure 5a). These surfaces are clearly inset into Q2 surfaces, are characterized by plumose texture caused by bar and swale surface morphology, and appear yellow-tan to tan-white in aerial photographs.

[19] The youngest surface, Q4, cuts all other surfaces and is composed of active and recently active channels (Figure 5a). These surfaces contain recent debris flow deposits, are relatively densely vegetated at the mouth of canyons with year-round water flow, but nearly devoid of vegetation far from the range front. These surfaces appear nearly white in aerial photographs.

[20] Two landslide deposits, unit Qls, are exposed at the range front and are composed of Paleozoic strata and Mesozoic intrusive rocks. The lobate morphology of the landslides is distinctive and the source area is characterized by a concave up escarpment. The two landslides were deposited across the main trace of the EIFZ.

[21] Locally exposed along the EIFZ-defined range front is unit Qc, an unconsolidated, generally medium to coarse grained sand and pebble-sized colluvium that often covers the range front fault scarp. Small dunes of medium- to fine-grained sand define unit Qs.

5. Fault Geometry, Geomorphology, Magnitude of Offset, and Slip Rates

[22] The EIFZ consists of two major geometric segments that connect the northern termination of the Hunter Mountain fault [e.g., *Burchfiel et al.*, 1987; *Oswald and Wesnousky*, 2002] with NE-striking normal faults that cut the Saline Range [*Sternlof*, 1988], thereby defining a right step within a dextral fault system; Saline Valley defines the pull-apart basin at that right step [e.g., *Burchfiel and Stewart*, 1966; *Oswald and Wesnousky*, 2002] (Figure 3). Recent slip along the EIFZ is inferred by the well-developed and fresh landforms, such as triangular facets, wineglass-shaped drainages, small alluvial fan size at the range front, fault scarps developed across young alluvial fans (Figure 5b), vertically offset drainages, and a steep range-front escarpment, up to 39° just north of McElvoy Canyon (Figure 2).

[23] Segment A of the EIFZ bounds the steep eastern flank of the Inyo Mountains (Figures 2 and 3). Here, the main trace of the EIFZ extends along strike for 24 km from Daisy Canyon to Willow Creek. This N26°W striking, E-dipping, dominantly normal fault zone is composed of bedrock fault planes and fault scarps cutting alluvial fan deposits. Basement rocks are exposed primarily within the footwall of the fault and Quaternary alluvial fan deposits are exposed primarily in the hanging wall. The height of the footwall escarpment above the valley floor is impressive ranging from ~2.5 km at Willow Creek to ~3.0 km at McElvoy Canyon (Figure 2). Gravity data indicate that maximum depth to basement in Saline Valley is 4.0–4.5 km and located approximately east of the mouth of McElvoy Canyon [*Blakely and Ponce*, 2001]. These observations yield a minimum vertical offset of 7.0–7.5 km across segment A. The fault along segment A is locally defined by a several m wide zone of extensively sheared, crushed, and fractured bedrock and up to a 1.5 m wide zone of bedrock-derived cataclasite and fault gouge. Fault surfaces and fault striae are exposed locally either within bedrock or at the bedrock/alluvial fan interface. The dip of the fault plane varies from 32 to 83° to the east; the average orientation is a 58° dip toward 82° (Figure 6). Fault striations, defined by grooves and small mullions, show a wider range in orientation and average a trend and plunge of 117°, 50° (Figure 6). Note that fault slip varies from dip slip normal to dextral oblique slip. Using the fault kinematic analysis method of *Marrett and Allmendinger* [1990], fault slip data from the EIFZ yield nearly horizontal E–W extension (azimuth of 99° and plunge of 10°, Figure 6).

[24] Primarily west-facing, discontinuous fault scarps cut and offset Q2b surfaces, but not Q3 and Q4 surfaces, along the southern two-thirds of segment A. Where these scarps cut and offset debris flow levees, field observations indicate both a vertical and dextral component of slip. At the mouth of McElvoy Canyon, a NNW-striking, W-facing fault scarp obliquely offsets several debris flow levees on a Q2b surface (Figures 7a and 8). Differential GPS surveying of

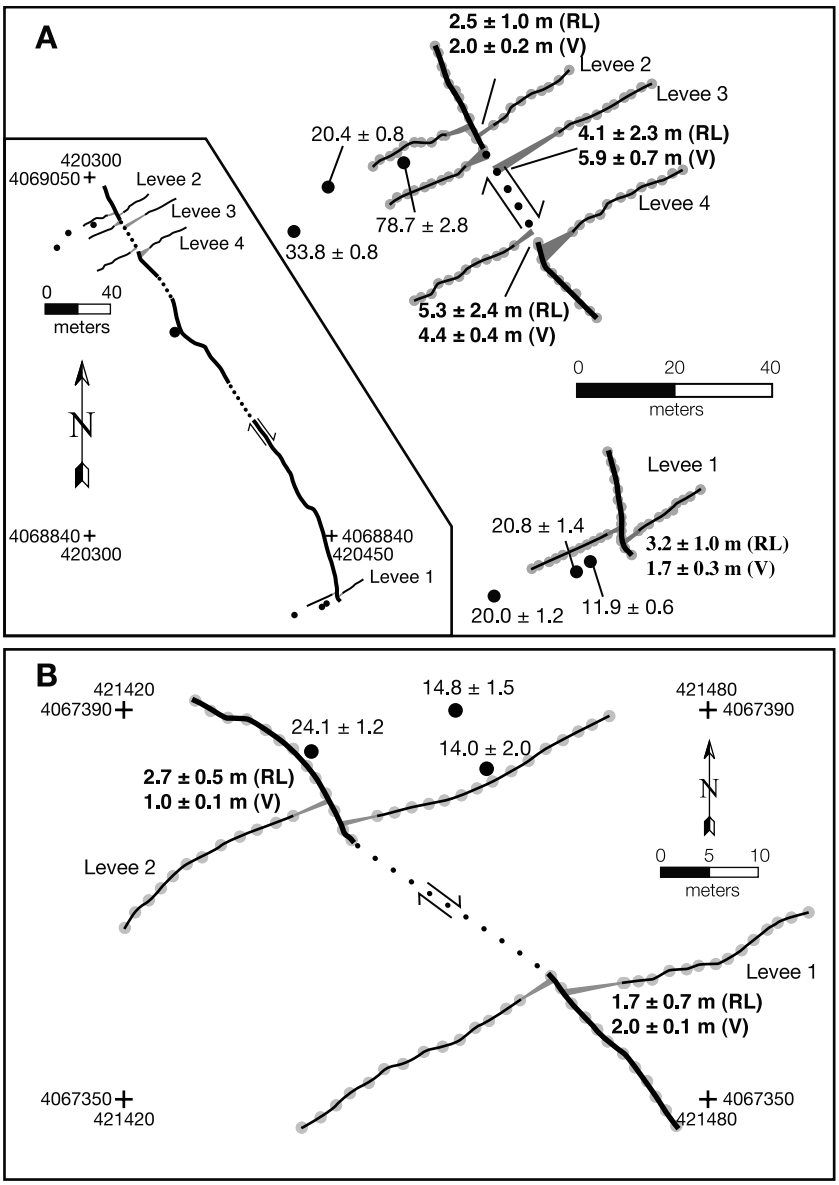

Figure 7. Simplified differential GPS maps showing fault scarp trace and offset levee apices developed within Q2b surfaces and TCN sample locations for (a) McElvoy Canyon and (b) a Q2b surface ~2 km south of McElvoy Canyon. Magnitude of right lateral strike-slip (RL) and vertical offset (V) shown. Differential GPS survey points indicated by gray circles; fault traces by thick black lines; levee apices by thin black lines; projection of levee apices by gray triangles; arrows indicate relative motion across faults; black circles indicate TCN sample locations; TCN ages are indicated by italic fonts. Universal transverse Mercator Zone 11 coordinates are World Geodetic System 84.

offset debris flow levee apices yields a weighted mean dextral offset of 3.1 ± 0.7 m and vertical offset of 2.4 ± 0.2 m, likely the result of a single earthquake. Assuming a fault dip of 50–70° yields horizontal extension of 1.5 ± 0.7 m and an oblique slip offset of 3.4 ± 0.7 m at 353 ± 12° since the abandonment of this surface at 18.3 ± 4.4 ka.

[25] A NW-striking, SW-facing fault scarp cuts another Q2b surface at ~2 km SE of McElvoy Canyon (Figure 7b). Here, differential GPS surveying of debris flow levee apices yields a weighted mean dextral offset of 2.4 ± 0.4 m and vertical offset of 1.5 ± 0.1 m. Assuming a fault dip of 50–70° yields horizontal extension of 0.9 ± 0.4 m and an oblique slip offset of 2.6 ± 0.4 m at 331 ± 9° since the abandonment of this surface at 17.7 ± 5.9 ka. Relatively fresh appearing bedrock fault scarps to the west of this fault scarp suggests that here, at least, recent fault slip is partitioned at the alluvial fan/bedrock interface and within alluvial fan deposits.

[26] Segment B of the EIFZ extends from Willow Creek northeastward (Figure 3). In this area, the EIFZ changes

Figure 8. View looking NNW at the SW-facing fault scarp cutting a Q2b surface at McElvoy Canyon. Main trace of the EIFZ and exhumed Inyo Mountain footwall block in the background.

from a relatively narrow fault zone at the base of the Inyo Mountains to ~15 km wide zone of ~N10–60°E striking, dominantly SE-dipping, but also NW-dipping, normal faults and fault scarps that cut pre-Tertiary rocks, Tertiary basalt lavas and gravels, and late Quaternary alluvial fan surfaces (Figures 3 and 5). Most fault scarps are well exposed in Q2a surfaces, but are locally exposed in Q3 surfaces, and absent across Q4 surfaces (Figure 5a). Fault scarps define SE- and NW-facing scarps, grabens, and nested grabens. Where fault scarps offset small debris flow channels or erosional escarpments cut into alluvial fan surfaces, geomorphic evidence indicates normal dip slip, but no dextral slip. Most scarps are mildly to moderately eroded and degraded, and sparsely vegetated (Figure 5b). In profile, fault scarp morphology varies from relatively short scarps with a single sharp knickpoint suggesting that these scarps formed by a single earthquake event to relatively tall, rounded scarps with more than one knickpoint suggesting that multiple earthquake events resulted in their formation. Where a single scarp can be traced from Q2 to Q3, that fault exhibits progressive offset with a larger vertical offset preserved within the Q2 surface. Our measured vertical offsets across scarps ranges from 0.02 to 8.98 m. Seven transects across fault scarps developed in Q2a surfaces yield a net minimum horizontal extension (assuming a fault dip of 60°) of from 2.8 ± 0.8 m to 14.3 ± 1.4 m (Figure 3 and Table 2). These measurements, combined with the ^{10}Be TCN model Q2a surface age of 44.3 ± 12.1 ka, yields a minimum horizontal slip rate of ~0.1–0.4 mm/a.

6. Zircon and Apatite (U-Th)/He Thermochronometry

[27] To document the low-temperature cooling history of granitic rocks exposed in the footwall of the EIFZ, 24 samples were collected from the Mesozoic Pat Keyes pluton across the central part of the Inyo Mountains (Figures 4 and 9). Samples were collected from a range of intrusive lithologies including quartz monzonite to monzonite-granodiorite, aplite dike, and diorite. (U-Th)/He zircon and apatite age results are summarized in Table 3 and Figures 9 and 10.

[28] (U-Th)/He zircon ages along the western flank of the range and the top half of the eastern flank yield an elevation invariant mean age of 65.8 ± 7.1 Ma (2σ) (Figures 9 and 10), an age consistent with late Cretaceous/early Tertiary cooling, regional exhumation of the Sierra magmatic arc, or Laramide deformation [e.g., *House et al.*, 1997, 2001; *Stockli et al.*, 2003; *Clark et al.*, 2005; *Bartley et al.*, 2007]. (U-Th)/He zircon ages from the middle part of the eastern flank of the range decrease down elevation from ~66 to ~54 Ma defining a Paleocene zircon partial retention zone (ZrPRZ). Below this inflection point, samples yield elevation invariant (U-Th)/He zircon ages of 55.0 ± 9.8 Ma over a present-day vertical distance of ~500 m. The two lowest elevation samples on the east side of the range yield ages similar to those in the ZrPRZ, but older than samples just above. This geometric age relation suggests that these two samples are in the hanging wall of a normal fault sliver that has duplicated, in part, the Eocene ZrPRZ. Although a fault to the west of these samples has been mapped (Figure 4), the absence of appropriate geologic markers make it impossible to confirm the magnitude of this inferred offset, nevertheless duplication of apatite fission track data [e.g., *Fitzgerald*, 1992; *Foster and Gleadow*, 1996] and (U-Th)/He data [*Stockli et al.*, 2003] have been used to estimate the magnitude of normal fault offset.

[29] (U-Th)/He apatite ages along the western flank of the range from its base to the range crest yield an elevation invariant mean age of 53.2 ± 6.6 Ma (Figures 9 and 10), an age also consistent with late Cretaceous/early Tertiary cooling, regional exhumation of the Sierra magmatic arc, or Laramide deformation [e.g., *House et al.*, 1997, 2001; *Stockli et al.*, 2003; *Clark et al.*, 2005; *Bartley et al.*, 2007]. Apatite (U-Th)/He ages from deeper structural levels exposed on the east side of the range define two exhumed apatite partial retention zones (APRZs) and inflection points (Figures 9 and 10). From the crest of the range, ages systematically decrease down the east side from ~53 Ma to ~16 Ma defining an Eocene-Miocene APRZ. Below this upper inflection point, samples yield elevation invariant (U-Th)/He ages of 15.6 ± 2.4 Ma over a present-day vertical

Table 2. Measured Horizontal Offsets and Calculated Slip Rates Across Normal Fault Scraps That Cut Dated Alluvial Fan Surfaces Along Transects Parallel to the Extension Direction[a]

Transect	Alluvial Fan Surface	Minimum Horizontal Offset (m)[b]	Surface Age (ka)	Horizontal Extension Rate (mm/a)
1	Qf2a	11.6 ± 1.3	44.3 ± 12.1	0.3 ± 0.1
2	Qf2a	7.3 ± 1.2	44.3 ± 12.1	0.2 ± 0.1
3	Qf2a	11.2 ± 1.7	44.3 ± 12.1	0.3 ± 0.1
4	Qf2a	14.3 ± 1.4	44.3 ± 12.1	0.3 ± 0.1
5	Qf2a	13.4 ± 1.3	44.3 ± 12.1	0.3 ± 0.1
6	Qf2a	13.4 ± 1.6	44.3 ± 12.1	0.3 ± 0.1
7	Qf2a	2.8 ± 0.8	44.3 ± 12.1	~0.1

[a]See Figure 3 for location of transects.
[b]Assumes 60° fault.

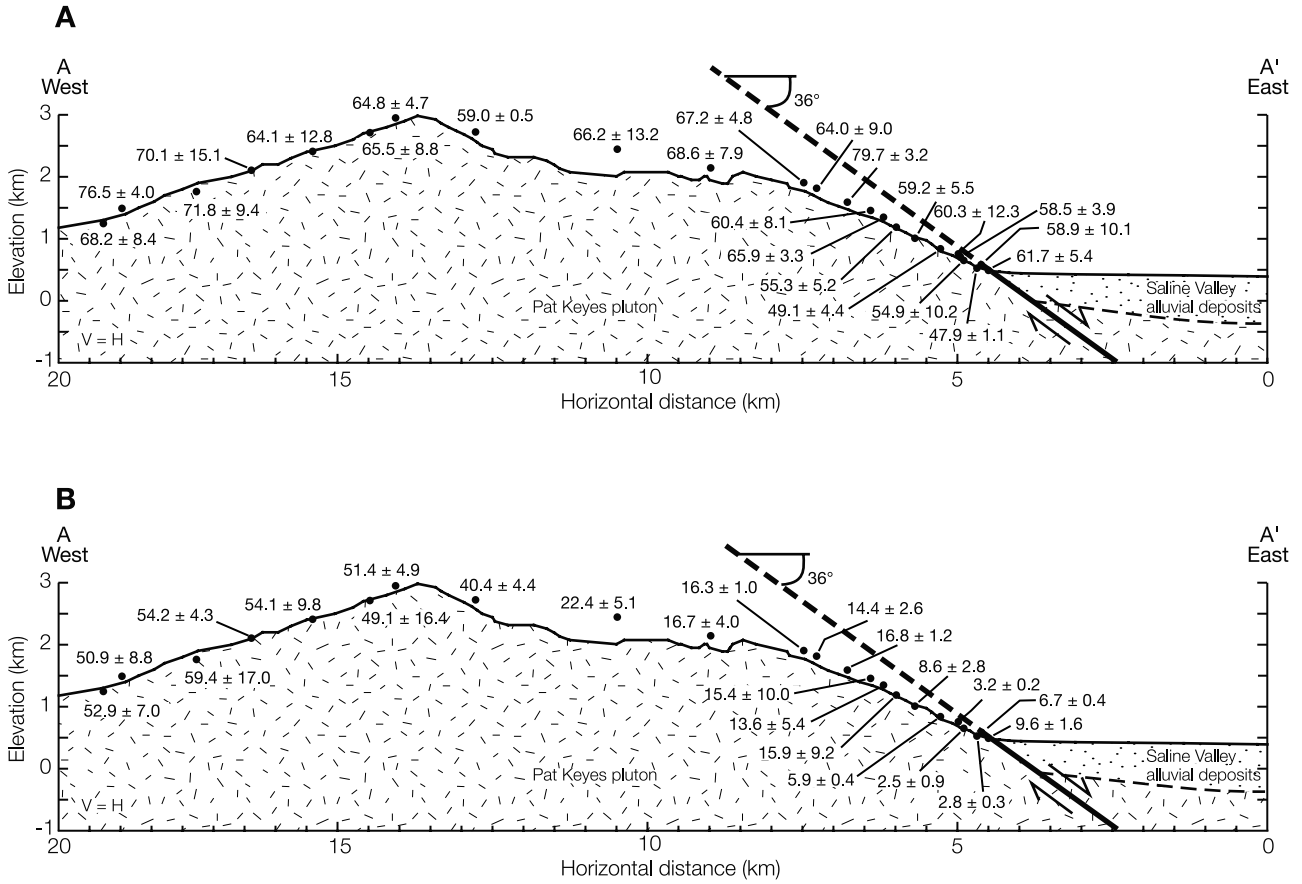

Figure 9. (a) Zircon and (b) apatite (U-Th)/He ages projected onto an EW cross section across the Inyo Mountains. Location of cross section shown in Figure 4.

distance of ~1000 m. (U-Th)/He ages then decrease again from ~15 Ma to ~3 Ma defining a Miocene-Pliocene APRZ. Below this lower inflection point, at the range front, samples yield elevation invariant ages of 2.8 ± 0.7 Ma over a present-day vertical distance of ~75 m. The two lowest elevation apatite samples on the east side of the range yield ages similar to the Miocene-Pliocene PRZ, but older than the age invariant samples just above. This geometric age relation, similar to the one documented for the lowest elevation zircon samples, suggests that these two samples are in the hanging wall of a normal fault sliver that has duplicated, in part, the Miocene-Pliocene PRZ.

[30] We interpret the zircon and apatite age patterns as indicating (Figure 10) (1) moderate to rapid cooling and exhumation at ~66 Ma; (2) slow cooling (<0.1 mm/a) and exhumation through the ZrPRZ between ~66 and ~55 Ma; (3) moderate to rapid cooling and exhumation at ~54 Ma; (4) slow cooling (<0.1 mm/a) through an older APRZ at high structural levels between ~53.0 and 15.6 Ma; (5) rapid cooling, exhumation, and initiation of normal slip, accommodated by westward tilting, along the EIFZ at 15.6 Ma; (6) a second episode of slow cooling (<0.1 mm/a) between 15.6 and 2.8 Ma through a younger APRZ; and (7) a second episode of rapid cooling, exhumation, and renewed normal slip along the EIFZ, and initiation of dextral slip along the Hunter Mountain fault at 2.8 Ma (see below).

[31] Tertiary sedimentary rocks are not exposed within the central part of the Inyo Mountains, therefore we cannot directly measure the degree of westward tilt that accumulated during Miocene to Present normal slip along the EIFZ. We can, however, estimate tilt magnitude by constraining the geothermal gradient. Zircon samples from the lowest elevations along the eastern flank and apatite samples along the western flank of the range from its base to the range crest yield the same age, ~54.1 Ma, within error (Figures 9 and 10). Therefore, at ~54.1 Ma eastern flank zircon samples were exhumed through the ZrPRZ, western apatite samples were exhumed through the APRZ, and all but two samples from the middle were between the two PRZs (Figure 11a). Only a 15°/km geothermal gradient satisfies these criteria. This geothermal gradient is similar (±5°) to an early Tertiary, preextensional geothermal gradient of ~15°C/km documented in the White Mountains, an east-tilted normal fault block and the northern continuation of the Inyo Mountains [*Stockli et al.*, 2003], as well as in other major normal fault blocks including the Sierra Nevada and Singatse Range [*Dumitru*, 1990; *House et al.*, 1997; *Surpless et al.*, 2002].

Table 3. Summary of Zircon and Apatite (U-Th)/He Sample Parameters, Analytical Data, and Mean Age for Samples Collected Across the Inyo Mountains[a]

Sample	Latitude[b]	Longitude[b]	Elevation (m)	Mass (mg)	He (ncc/mg)	U (ppm)	Th (ppm)	Ft	Mean Age (Ma)	$\pm 2\sigma$[c] (Ma)	Replicates[d]
Zircon in the Eastern Range Flank											
IM950	36°45.402′	118°00.034′	3015	8.5	65.4	210.9	115.3	0.78	64.8	4.7	3
IM900E	36°45.786′	117°59.226′	2745	5.0	56.5	201.2	142.0	0.76	59.0	0.5	3
IM800E	36°46.488′	117°57.806′	2444	4.6	152.4	507.1	326.2	0.74	66.2	13.2	3
IM700E	36°46.752′	117°56.838′	2153	5.3	59.1	180.1	125.9	0.76	68.6	7.9	3
IM620E	36°47.184′	117°55.887′	1895	5.2	44.6	144.1	76.4	0.75	67.2	4.8	3
IM580E	36°47.162′	117°55.740′	1771	6.7	76.0	260.0	123.0	0.77	64.0	9.0	3
IM530E	36°47.240′	117°55.419′	1616	5.3	61.1	163.0	106.1	0.75	79.7	3.2	3
IM460E	36°47.219′	117°55.123′	1422	4.1	42.4	151.9	93.1	0.74	60.4	8.1	3
IM430E	36°47.174′	117°55.012′	1315	6.4	57.9	179.3	135.5	0.77	65.9	3.3	3
IM380E	36°47.172′	117°54.830′	1157	5.6	31.1	120.6	59.9	0.77	55.3	5.2	3
IM330E	36°47.153′	117°54.610′	1009	8.3	35.7	122.5	75.1	0.79	59.2	5.5	3
IM280E	36°47.016′	117°54.330′	870	5.3	60.0	281.0	66.2	0.76	49.1	4.4	3
IM230E	36°47.021′	117°54.152′	713	21.3	30.2	96.2	83.5	0.83	60.3	12.3	3
IM220E	36°47.033′	117°54.100′	670	4.4	120.8	437.3	300.7	0.75	58.5	3.9	3
IM210EB	36°45.480′	117°53.880′	640	7.0	76.2	292.9	157.1	0.77	54.9	10.2	3
IM210EA	36°45.444′	117°53.620′	661	3.8	21.8	100.8	63.6	0.73	47.9	1.1	3
IM170BE	36°46.894′	117°53.915′	520	5.8	62.7	212.5	146.9	0.76	61.7	5.4	3
IM170AE	36°46.894′	117°53.915′	520	4.3	61.0	223.8	141.1	0.73	58.9	10.1	3
Zircon in the Western Range Flank											
IM900W	36°45.734′	118°00.397′	2751	5.3	102.8	324.4	187.1	0.76	65.5	8.8	3
IM800W	36°45.646′	118°01.008′	2457	3.2	82.7	300.9	123.3	0.72	64.1	12.8	3
IM700W	36°45.749′	118°01.708′	2157	8.0	101.0	306.5	193.0	0.75	70.1	15.1	3
IM600W	36°45.606′	118°02.287′	1813	23.4	67.8	173.9	145.2	0.84	71.8	9.4	3
IM500W	36°45.662′	118°03.116′	1542	9.1	74.3	199.7	156.1	0.77	76.5	4.0	3
IM430W	36°45.182′	118°03.213′	1317	3.8	150.0	452.8	463.1	0.72	68.2	8.4	2
Apatite in the Eastern Range Flank											
IM950	36°45.402′	118°00.034′	3015	3.5	140.0	20.1	68.7	0.64	51.4	4.9	2
IM900E	36°45.786′	117°59.226′	2745	1.6	70.4	11.9	48.9	0.61	40.4	4.4	4
IM800E	36°46.488′	117°57.806′	2444	7.6	67.6	16.3	75.7	0.72	22.4	5.1	4
IM700E	36°46.752′	117°56.838′	2153	3.0	122.1	29.8	126.4	0.66	16.7	4.0	3
IM620E	36°47.184′	117°55.887′	1895	2.4	56.6	25.4	68.0	0.63	16.3	1.0	1
IM580E	36°47.162′	117°55.740′	1771	2.7	76.6	57.0	62.2	0.61	14.4	2.6	2
IM530E	36°47.240′	117°55.419′	1616	3.1	83.8	29.9	76.0	0.65	16.8	1.2	2
IM460E	36°47.219′	117°55.123′	1422	3.9	62.1	44.0	5.5	0.69	15.4	10.0	2
IM430E	36°47.174′	117°55.012′	1315	4.7	46.1	38.5	9.1	0.67	13.6	5.4	2
IM380E	36°47.172′	117°54.830′	1157	3.3	79.8	35.2	52.0	0.64	15.9	9.2	3
IM330E	36°47.153′	117°54.610′	1009	2.4	45.9	71.9	7.8	0.63	8.6	2.8	2
IM280E	36°47.016′	117°54.330′	870	2.9	20.6	43.0	8.8	0.64	5.9	0.4	2
IM230E	36°47.021′	117°54.152′	713	4.4	15.9	38.0	76.4	0.73	3.2	0.2	1
IM210EB	36°45.480′	117°53.880′	640	3.8	11.4	45.3	58.2	0.65	2.5	0.9	2
IM210EA	36°45.444′	117°53.620′	661	1.4	13.4	51.4	50.3	0.62	2.8	0.3	2
IM170BE	36°46.894′	117°53.915′	520	3.1	86.5	94.5	95.0	0.64	9.6	1.6	2
IM170AE	36°46.894′	117°53.915′	520	3.7	9.3	11.7	24.2	0.66	6.7	0.4	1
Apatite in the Western Range Flank											
IM900W	36°45.734′	118°00.397′	2751	3.0	131.9	18.4	69.0	0.63	49.1	16.4	2
IM800W	36°45.646′	118°01.008′	2457	3.9	198.3	31.8	81.1	0.67	54.1	9.8	3
IM700W	36°45.749′	118°01.708′	2157	5.7	355.9	71.9	61.3	0.70	54.2	4.3	3
IM600W	36°45.606′	118°02.287′	1813	2.2	249.4	51.9	56.5	0.61	59.4	17.0	2
IM500W	36°45.662′	118°03.116′	1542	2.0	155.1	35.1	33.2	0.59	50.9	8.8	4
IM430W	36°45.182′	118°03.213′	1317	2.0	124.2	23.0	28.5	0.65	52.9	7.0	2

[a]See Figures 4 and 9 for location of samples.
[b]World Geodetic System 84 datum.
[c]Errors on single replicate analyses are 6 percent (2σ) and are the analytical uncertainty on laboratory internal reproducibility.
[d]Number of replicates per sample. See Auxillary Material A for replicate analyses.

[32] To place bounds on the exhumation history and degree of westward tilt in the Inyo Mountains, we restored sample positions using the following:

[33] 1. Our estimated preextensional, late Cretaceous/early Tertiary geothermal gradient of 15°C/km and a mean annual surface temperature of 10°C. We assume a linear geothermal gradient, which is probably reasonable for shallow crustal levels [e.g., *Stockli et al.*, 2002], but likely not so at deep structural levels.

[34] 2. A preextensional middle Miocene geothermal gradient of 15°C/km, similar to the middle Miocene geo-

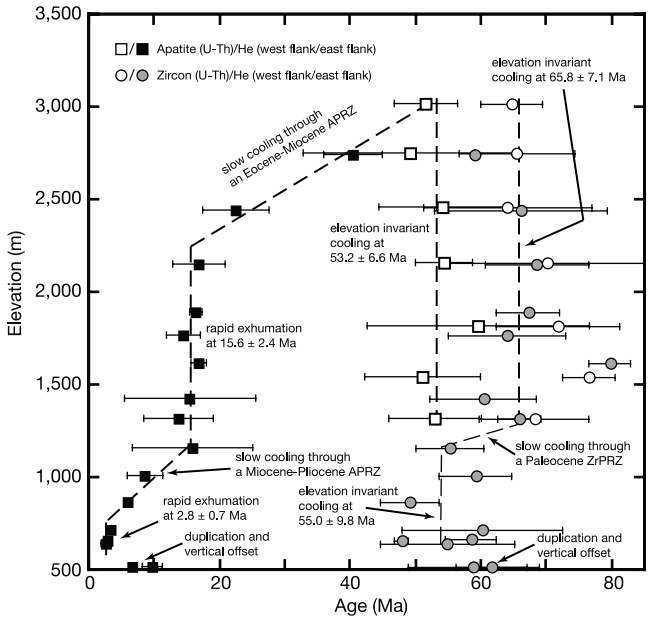

Figure 10. Plot of zircon and apatite (U-Th)/He ages versus elevation showing the cooling history for the Inyo Mountains.

thermal gradient documented in the White Mountains [*Stockli et al.*, 2003].

[35] 3. An increase in geothermal gradient to 35°C/km during the Pliocene, as has been documented in the Wassuk Range [*Stockli et al.*, 2002]. The extensive Pliocene basalt and andesite lavas exposed along the eastern flank of the Inyo Mountains and in the Saline Range [*Ross*, 1970; *Larsen*, 1979; *Elliot et al.*, 1984; *Sternlof*, 1988], as well as the six heat flow sites in Saline Valley, which yield a near surface mean geothermal gradient of 38°C/km, suggest that this increase in geothermal gradient is reasonable. If we minimize the magnitude of late Cretaceous/early Paleocene tilt of the Inyo Mountains, then its low-temperature exhumation history began at ~66 with at least 7.5 km of slow to rapid (≥0.5 mm/a) exhumation through the ZrPRZ (Figure 11a). Between ~66 and ~54 Ma, little or no significant exhumation occurred. At ~54.1 Ma, the Inyo Mountains were moderately to rapidly exhumed (≥0.8 mm/a) ~3.9 km and tilted 12°eastward through the APRZ (Figure 11a). Between ~54 Ma and ~16 Ma, the Inyo Mountains were essentially static. The rapid (≥ 1.9 mm/a) episode of exhumation at ~15.6 Ma was characterized by ~16° of westward tilt and exhumation of the eastern flank by ~5.3 km through the APRZ (Figure 11a). Between ~15.6 and ~2.8 Ma, the Inyo Mountains were characterized by slow exhumation (0.1–0.2 mm/a) and 4° of westward tilt. This period was followed by an increase in the geothermal gradient to 35°C/km and onset of somewhat faster exhumation (0.4–0.7 mm/a), ~4° of westward tilt, and 1.5 km exhumation of the eastern flank of the range through the upper part of the APRZ at ~2.8 Ma (Figure 11a).

[36] Alternatively, the reconstructions yield a somewhat different early exhumation history if we minimize the magnitude of the late Cretaceous/early Paleocene exhumation (Figure 11b). In this scenario, the Inyo Mountains were exhumed ~6.4 km at a slow to rapid rate (≥0.5 mm/a) at ~66 Ma. This was followed by a period of stasis between ~66 and ~54 Ma and then a period of significant exhumation (~5.6 km) at a rate of ≥1.1 mm/a accompanied by 20° eastward tilt at ~54.1 Ma. The younger history of exhumation follows that described above (Figure 11a).

[37] In summary, zircon and apatite (U-Th)/He data indicate four major episodes of moderate to rapid exhumation and tilting: (1) a late Cretaceous/early Paleocene episode of 6.4–7.5 km of exhumation; (2) an early Eocene episode of 3.9–5.6 km of exhumation; (3) a middle Miocene episode of rapid cooling, ~5.3 km of exhumation, and 16° of westward tilt; and (4) a Pliocene to Recent episode of renewed rapid cooling, ~1.5 km of exhumation, and 4° of westward tilt. In addition, the (U-Th)/He data indicate a protracted episode (~40 Ma) of stasis from the early Eocene to middle Miocene. Exhumation of the Inyo Mountains commenced in the late Cretaceous/early Tertiary along structure(s) that have not yet been identified. This period of exhumation was followed by a prolonged phase of slow erosion which ended with two late Tertiary episodes of exhumation and westward tilting along the down to the east normal slip EIFZ (see below).

[38] We can calculate the magnitude of downdip slip along the EIFZ since inception of slip at ~15.6 Ma using an estimate of ~8.5 km of vertical exhumation (based on a geothermal gradient of 15°C/km) for the eastern most samples, 24° of westward tilt (Figure 11a), and assuming an initial fault dip of 60 ± 10°. These constraints yield downdip normal slip and horizontal extension amounts of between 9.8 +1.3/–0.8 (60 ± 10° dipping fault) and 14.5 +4.9/–2.7 (36 ± 10° dipping fault) km, and between 4.9 +2.2/–1.8 and 11.7 +5.7/–3.5 km, respectively. Combining the dip slip and horizontal extension measurements that accumulated since onset of extension at 15.6 ± 2.4 Ma yields a middle Miocene dip slip rate of between 0.6 ± 0.1 and 0.9 +0.4/–0.2 mm/a and horizontal extension rate of between 0.3 +0.2/–0.1 and 0.8 +0.4/–0.2 mm/a.

7. Discussion

7.1. Late Cretaceous/Early Tertiary Exhumation

[39] Late Cretaceous to early Tertiary apatite fission track and (U-Th)/He ages have been documented in several normal fault blocks in the western Basin and Range Province including the Sierra Nevada, White Mountains, Wassuk Range, Singatse Range, Pine Nut Mountains, and Carson Range [*Dumitru*, 1990; *House et al.*, 1997, 2001; *Stockli et al.*, 2002, 2003; *Surpless et al.*, 2002; *Clark et al.*, 2005]. These ages have been interpreted as either refrigeration during shallow Laramide subduction [*Dumitru*, 1990], cooling of the Sierra Nevada magmatic arc [*Stockli et al.*, 2003], or protracted late Cretaceous-early Tertiary erosional unroofing [*House et al.*, 1997; *Stockli et al.*, 2002; *Surpless et al.*, 2002; *Clark et al.*, 2005].

[40] The two episodes of late Cretaceous/early Tertiary moderate to rapid exhumation and tilting of the Inyo

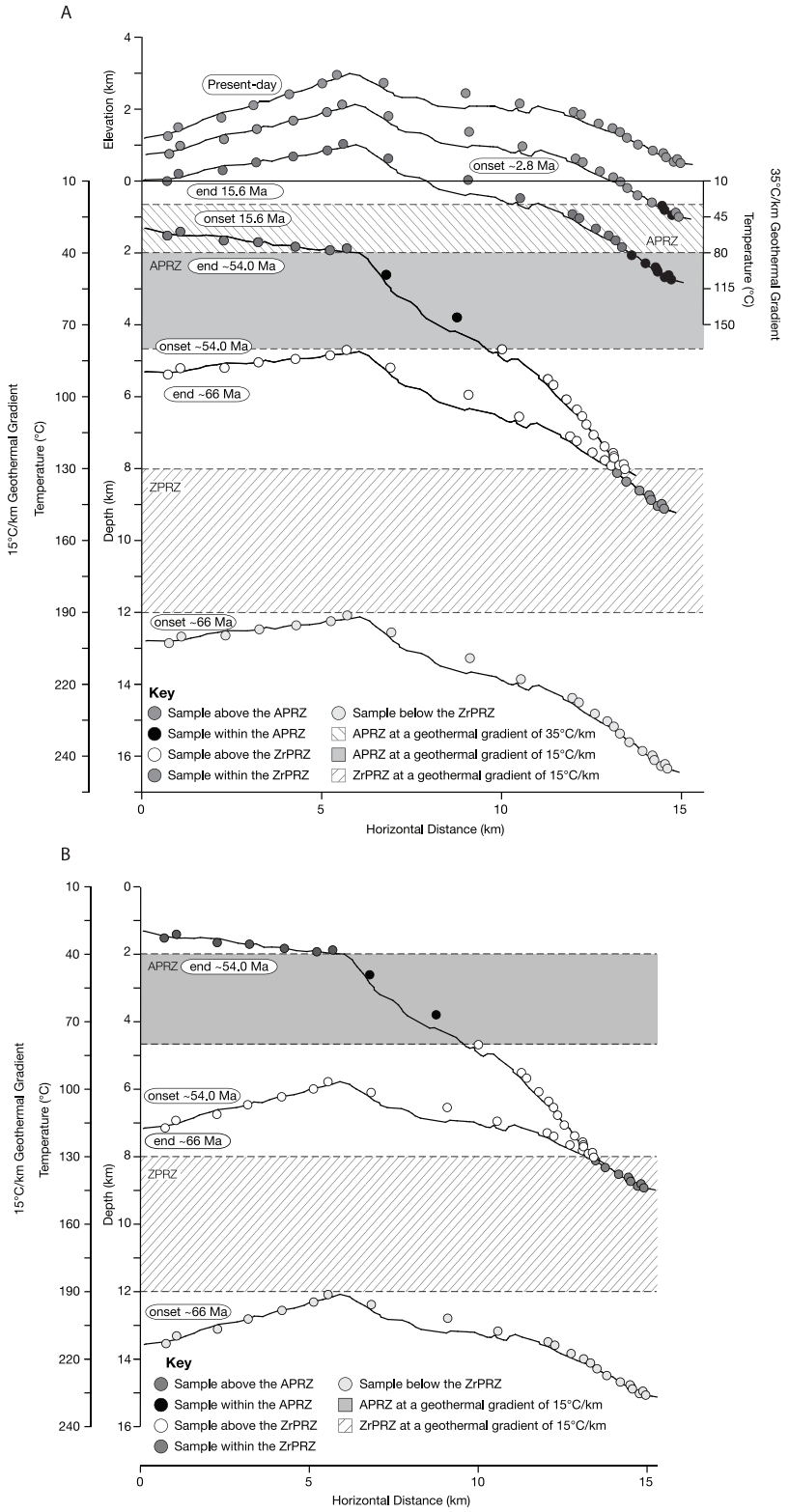
A
Elevation (km)
Present-day
onset ~2.8 Ma
end 15.6 Ma
onset 15.6 Ma
APRZ
APRZ end ~54.0 Ma
onset ~54.0 Ma
end ~66 Ma
ZPRZ
onset ~66 Ma
35°C/km Geothermal Gradient
Temperature (°C)
15°C/km Geothermal Gradient
Temperature (°C)
Depth (km)
Horizontal Distance (km)
Key
Sample above the APRZ
Sample within the APRZ
Sample above the ZrPRZ
Sample within the ZrPRZ
Sample below the ZrPRZ
APRZ at a geothermal gradient of 35°C/km
APRZ at a geothermal gradient of 15°C/km
ZrPRZ at a geothermal gradient of 15°C/km
B
APRZ end ~54.0 Ma
onset ~54.0 Ma
end ~66 Ma
ZPRZ
onset ~66 Ma
15°C/km Geothermal Gradient
Temperature (°C)
Depth (km)
Horizontal Distance (km)
Key
Sample above the APRZ
Sample within the APRZ
Sample above the ZrPRZ
Sample within the ZrPRZ
Sample below the ZrPRZ
APRZ at a geothermal gradient of 15°C/km
ZrPRZ at a geothermal gradient of 15°C/km

Figure 11

Mountains are not compatible with either of these interpretations but are broadly similar in time with Laramide deformation. *Wells and Hoisch* [2008, and reference therein] summarize several studies that suggest extension was widespread throughout the interior of the Laramide orogeny, however the timing of that deformation is generally not well defined. In the vicinity of the Inyo Mountains, the best geochronologic constraints on Laramide deformation come from the Funeral and Black mountains and across Owens Valley, the valley bounding the western flank of the Inyo Mountains. In the Funeral Mountains, field and U/Pb zircon geochronologic data show a major extensional unroofing event that was ongoing at 72 ± 1 Ma and ceased by 70 ± 1 Ma [*Applegate et al.*, 1992], prior to the low-temperature exhumation history recorded in the Inyo Mountains. Field and geochronologic data from the Black Mountains, located ~55 km south of the Funeral Mountains, indicate an episode of contractional deformation between 61 and 55 Ma [*Miller and Friedman*, 1999; *Miller and Pavlis*, 2005; *Miller*, 2003], approximately the same time as the two episodes of exhumation recorded in the Inyo Mountains. Across Owens Valley, ~65 km of dextral offset is indicated by the $^{87}Sr/^{86}Sr = 0.706$ isotopic isopleth in the Mono Lake area, a Middle Devonian submarine channel, Permo-Triassic structures, and the late Cretaceous Golden Bear dike/Coso dikes [*Kistler*, 1993; *Stevens et al.*, 1997; *Kylander-Clark et al.*, 2005]. The timing of offset postdates the emplacement of the Golden Bear and Coso dikes at ~83 Ma [*Kylander-Clark et al.*, 2005]. *Bartley et al.* [2007] and *Glazner et al.* [2005] suggested that as much as 50–60 km of the dextral offset accumulated during the late Cretaceous to early Tertiary (Laramide time). Furthermore, *Bartley et al.* [2007] postulated that this episode of NW dextral slip was linked to an extensional step over in the southern Sierra Nevada, where *Wood and Saleeby* [1997] proposed ~90–85 Ma to ~55–50 Ma south to southeast extension along normal faults and an extensional detachment system that unroofed the southern Sierra Nevada batholith. We speculate that the two late Cretaceous/early Tertiary episodes of exhumation documented in the Inyo Mountains indicate two phases of Laramide deformation associated with dextral slip across Owens Valley.

[41] The early Eocene episode of rapid exhumation was followed by a prolonged period (~40 Ma) of quiescence. The lack of exhumation during this time period suggests development of a slowly eroding surface, as has been proposed for the Sierra Nevada between 80 and 32 Ma [*Clark et al.*, 2005], of which the Inyo Mountains were a part prior to the onset of late Tertiary extension.

7.2. Basin and Range Extension

[42] Geologic mapping, structural, and kinematic studies, combined with apatite (U-Th)/He thermochronometry, show that the EIFZ is characterized by two normal fault segments, an Inyo Mountain range bounding, NNW-striking, E-dipping normal to normal oblique slip fault and a broad zone of NE-striking normal fault scarps cutting across northern Saline Valley and projecting into the Saline Range (Figures 1, 2, and 3). Apatite (U-Th)/He thermochronometry results across the Inyo Mountains yield age patterns that indicate two periods of rapid cooling, exhumation, and normal slip. Normal slip initiated at 15.6 Ma and did not last for more than ~1.5 Ma as demonstrated by ≥13.62 ± 0.52 Ma alluvial fan sediments deposited across, but not cut by, the southeast extension of the EIFZ in the southern Inyo Mountains [*Conrad*, 1993]. A second episode of normal slip began at 2.8 Ma and fault scarps that cut late Pleistocene alluvial fan surfaces indicate the EIFZ is still active today.

[43] Middle Miocene initiation of normal slip along the EIFZ is similar in age to the initiation of normal slip and tilt documented along a number of major fault blocks to the north. Normal faulting and eastward tilt in the White Mountains began at ~12 Ma [*Stockli et al.*, 2003]. Farther to the north, large magnitude extension in the Yerington area and normal faulting and westward tilt of the Singatse and Wassuk Ranges started at 13–15 Ma [*Dilles and Gans*, 1995; *Stockli et al.*, 2002; *Surpless et al.*, 2002]. Normal faulting initiated at ~12 Ma along the east-dipping Donner Pass fault zone located within the eastern margin of the Sierra Nevada southwest of Reno, Nevada [*Henry and Perkins*, 2001]. These normal fault blocks define a 20°N–30°W-trending zone of middle Miocene, approximately NS-striking, west-stepping, en echelon normal faults along the western margin of the Basin and Range Province. If the southern part of the Sierra Nevada frontal fault zone was not active during the middle Miocene (but see below), then these fault blocks define a middle Miocene breakaway zone along the boundary between highly extended Basin and Range Province to the east from the unextended Sierra Nevada to west [*Surpless et al.*, 2002]. Middle Miocene extension in this region of the Basin and Range Province has been attributed to development of a slab window [e.g.,

Figure 11. (a) Restored positions of zircon and apatite (U-Th)/He samples using a late Cretaceous to middle Tertiary geothermal gradient of 15°C/km and a Pliocene to present geothermal gradient of 35°C/km and assuming horizontal isotherms (see text for discussion). This reconstruction minimizes the magnitude of tilt during the late Cretaceous/early Tertiary exhumation episode. Late Cretaceous to early Tertiary and middle Miocene zircon partial retention zone indicated by left-slanted line shading and apatite partial retention zone indicated by gray shading; Pliocene APRZ indicated by right-slanted line shading. Onset and end show sample positions at the beginning and cessation, respectively, of a period of rapid cooling and exhumation. (b) Restored positions of zircon and apatite (U-Th)/He samples using a late Cretaceous to middle Tertiary geothermal gradient of 15°C/km, horizontal isotherms, and a reconstruction that minimizes the magnitude of exhumation during the late Cretaceous/early Tertiary exhumation episode (cf. Figure 11a). The younger exhumation history is the same as in Figure 11a. ZrPRZ indicated by left slanted line shading and APRZ indicated by gray shading. Onset and end show sample positions at the beginning and cessation, respectively, of a period of rapid cooling and exhumation.

Atwater and Stock, 1998; *Dickinson*, 2002] or a combination of forces external to the region including plate boundary forces, an increased gravitational potential energy in the northern Basin and Range Province, and lateral forces in the southern Basin and Range Province [*Sonder and Jones*, 1999].

[44] The renewed episode of normal slip along the EIFZ during the Pliocene is also similar in age to the timing of renewed slip along many of the same fault systems to the north that experienced slip during the middle Miocene. Younger extension at the northern end of the White Mountains initiated at ~3 Ma [*Stockli et al.*, 2003], while renewed normal slip in the Wassuk Range began at<4 Ma [*Stockli et al.*, 2002]. Along the eastern margin of the Sierra Nevada west of Reno, extension restarted at ~3 Ma [*Henry and Perkins*, 2001], and the initiation of extension along the eastern margin of Sierra Nevada in the Tahoe-Truckee asymmetric half graben occurred after 5 Ma [*Surpless et al.*, 2002].

[45] A number of observations, including westward tilted Neogene strata [*Unruh*, 1991; *Wakabayashi and Sawyer*, 2001], high incision rates [*Stock et al.*, 2004], and the petrology, geochemistry, and geochronology of volcanic rocks and entrapped xenoliths [e.g., *Ducea and Saleeby*, 1996; *Farmer et al.*, 2002; *Manley et al.*, 2000; see also *Jones et al.*, 2004], suggest tectonic uplift and westward tilt of the Sierra Nevada west of the Inyo Mountains at 5–3.5 Ma. This episode of extension has been attributed to removal of dense lithosphere from beneath the Sierra Nevada at ~3.5 Ma that initiated uplift and increased extensional strain rates within a 50 km distance east of the Sierra Nevada [e.g., *Ducea and Saleeby*, 1996; *Jones et al.*, 2004; *Zandt et al.*, 2004]. The second, Pliocene, episode of normal slip along the EIFZ is consistent with this hypothesis.

[46] The absence of Cenozoic rocks that can be correlated across the Sierra Nevada and into Owens Valley and late Cenozoic low-temperature thermochronometry ages precludes directly dating initiation of slip along this section of the Sierra Nevada frontal fault zone. However, combining geomorphology and (U-Th)/He thermochronometry, *Clark et al.* [2005] concluded that the southern Sierra Nevada experienced an episode of exhumation between 32 and 3.5 Ma. Furthermore, combining a minimum vertical relief of ~2.5 km at the latitude of Mt. Whitney with the assumption that late Pleistocene to Holocene vertical slip rates of 0.2–0.3 mm/a along the Sierra Nevada frontal fault zone [*Le et al.*, 2007] have remained constant through time implies that the eastern escarpment here may be at least as old as ~9–13 Ma. Finally, Sierran derived sandstones, gravels, and boulders observed in ~8 Ma basin deposits along the southeastern most Sierra Nevada implies tectonic uplift at this time [*Loomis and Burbank*, 1988]. Although not conclusive, these observations suggest that normal slip along the Sierra Nevada frontal fault zone west of the Inyo Mountains was ongoing during the middle to late Miocene. If correct, then the Sierra Nevada frontal fault zone would have formed a breakaway zone with the west-tilted Inyo Mountains in its hanging wall.

7.3. Eastern California Shear Zone

[47] As extension shifted westward at the latitude of ~38.5° and ~36.5°, the rigid Sierra Nevada block became narrower [*Surpless et al.*, 2002; *Jones et al.*, 2004], and because it lies within a transform plate boundary, *Sonder and Jones* [1999] postulated that shear strain was localized along its boundaries. Thus, an increase in dextral shear at ~3.5 Ma is predicted within the ECSZ [*Jones et al.*, 2004], a hypothesis supported by the interpretation that initiation of normal slip along the NE-striking Queen Valley at 3.0 ± 0.5 Ma signals the onset of dextral slip along the Owens Valley-White Mountains fault zone [*Stockli et al.*, 2003]. Similarly, the Pliocene slip history along the EIFZ is related to the onset of dextral shear within the ECSZ.

[48] The northern termination of the dextral Hunter Mountain fault is defined by the EIFZ while the normal slip Panamint Valley fault defines the southern termination (Figure 1). The Saline and Panamint valleys are pull-apart basins in this right-stepping geometry. The EIFZ, therefore, transfers dextral slip from the Hunter Mountain fault to normal faults within the Saline Range and Dry Mountain, which, in turn, transfer slip across to the dextral Furnace Creek fault [e.g., *Dixon et al.*, 1995; *Lee et al.*, 2001]. As a consequence, the timing of Pliocene slip along the EIFZ has implications for the onset and rate of slip along the Hunter Mountain fault and for the total geologic slip rate across the ECSZ.

[49] The intersection line defined by a subhorizontal basalt flow capping a subvertical contact between the Hunter Mountain batholith and Paleozoic rocks is dextrally offset 9.3 ± 1.4 km across the Hunter Mountain fault [*Burchfiel et al.*, 1987; *Sternlof*, 1988]. This maximum measured dextral offset accumulated since 4.63 ± 0.06 Ma, the age of the youngest basalt flow, indicating a minimum dextral slip rate of 2.0 ± 0.3 mm/a [*Burchfiel et al.*, 1987; *Sternlof*, 1988]. *Sternlof* [1988] calculated 8.9 ± 2.5 km of horizontal extension across the Saline Range, the same, within error, as the dextral offset across the Hunter Mountain fault, supporting the kinematic configuration whereby the EIFZ transfers slip from the Hunter Mountain fault to NE-striking normal faults exposed in the Saline Range. *Sternlof* [1988] further argued that 4.5 ± 0.1 km of horizontal extension across the Saline Range can account for the dextral slip along the Hunter Mountain fault since 1.37 ± 0.01 Ma, yielding a minimum dextral slip rate of 3.2 ± 0.1 mm/a. These studies show that the initiation of dextral slip along the Hunter Mountain fault is bracketed between 4.6 and 1.4 Ma. Finally, *Oswald and Wesnousky* [2002] calculated a late Pleistocene dextral slip rate of 3.3–4.0 mm/a across the Hunter Mountain fault based on a 50–60 m dextrally offset drainage developed within an alluvial surface, whose geomorphic characteristics along with climate factors suggest is ~15 ka.

[50] We suggest that the episode of renewed normal slip along the EIFZ at 2.8 ± 0.7 Ma signals the onset of dextral slip along the Hunter Mountain fault and extension across the Saline Range because the EIFZ forms the northern termination of the Hunter mountain fault. If correct, then the total dextral offset of 9.3 ± 1.4 km along the Hunter

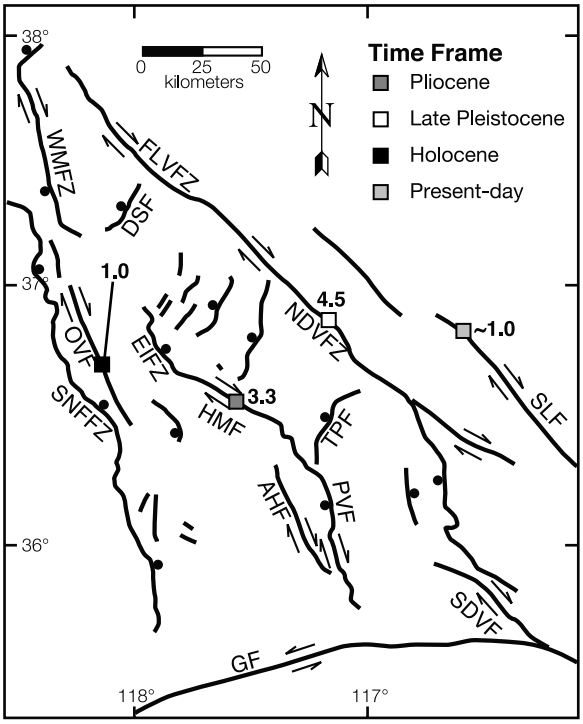

Figure 12. Simplified fault map of the eastern California shear zone showing active and recently active faults and geologically determined dextral slip rates in mm/a [*Bacon and Pezzopane*, 2007; *Frankel et al.*, 2007; *Guest et al.*, 2007; this work]. Squares indicate location of the calculated slip rate. AHF, Ash Hills fault; DSF, Deep Springs fault; EIFZ, eastern Inyo fault zone; FLVFZ, Fish Lake Valley fault zone; GF, Garlock fault; HMF, Hunter Mountain fault; NDVFZ, Northern Death Valley fault zone; OVF, Owens Valley fault; PVF, Panamint Valley fault; TPF, Towne Pass fault; SDVF, Southern Death Valley fault; SLF, Stateline fault; SNFFZ, Sierra Nevada frontal fault zone; WMFZ, White Mountains fault zone.

Mountain fault [*Sternlof*, 1988] accumulated at a rate of 3.3 ± 1.0 mm/a since the Pliocene. This long-term slip rate is the same, within error, as *Sternlof*'s [1988] calculated early Pleistocene dextral slip rate and *Oswald and Wesnousky*'s [2002] estimated latest Pleistocene slip rate. Our estimate for the age of initiation of dextral slip along the Hunter Mountain fault is the same, within error, to that for the Owens Valley-White Mountains fault zone [*Stockli et al.*, 2003], and consistent with *Jones et al.*'s [2004] hypothesis that dextral shear increased within the western part of the ECSZ during the Pliocene.

[51] Our calculated dextral slip rate along the Hunter Mountain fault, combined with calculated dextral slip rates for the other three major dextral strike-slip faults, the southern Owens Valley, northern Death Valley, and Stateline faults, provides an estimate of the cumulative slip rate across the ECSZ at the latitude of ~36.5° (Figures 1 and 12 and Table 4). A Holocene dextral slip rate of 1.0 ± 0.4 mm/a was estimated by *Bacon and Pezzopane* [2007] across the southern Owens Valley fault based on paleoseismic studies. *Frankel et al.* [2007] report a dextral slip rate of 4.2 +1.9/−1.1 to 4.7 +0.9/−0.6 mm/a across the northern Death Valley fault based on 297 ± 9 m offset of an alluvial fan surface with a maximum and minimum age of 70 +22/−20 ka and 63 ± 8 ka, respectively. Along the southern part of the Stateline fault, *Guest et al.* [2007] calculated a minimum middle Miocene dextral slip rate of 2.3 ± 0.1 mm/a based on 30 ± 1 km dextral offset of middle Miocene volcanic deposits. This slip rate is considerably higher than geodetic estimates of 0.7–1.2 mm/a [*Wernicke et al.*, 2004; *Hill and Blewitt*, 2006], which was measured across the northern part of the fault. *Guest et al.* [2007] postulated that one potential explanation for this discrepancy is an along strike change in displacement rate along the Stateline fault. The lower rate of ~1 mm/a on the northern segment may be the consequence of transfer of ~55% of the dextral slip from the southern segment northwestward onto the Death Valley fault via a left step.

[52] Summing geologic slip rates, calculated parallel to Pacific-North America plate motion (N47°W) [*Dixon et al.*, 2000], from the Owens Valley, northern Death Valley, and Stateline faults with the slip rate determined for the Hunter Mountain fault in this study and assuming slip rates were constant through time, yields a total long-term geologic slip rate of 9.3 +2.2/−1.4 to 9.8 +1.4/−1.0 mm/a (Figure 12 and Table 4). Our geologic slip rate estimate is the same as *Frankel et al.*'s [2007] recent geologic slip rate estimate, although they used a somewhat faster slip rate for the Owens Valley fault and did not calculate rates parallel to Pacific-North American plate motion. Our estimated long-term geologic slip rate is also the same, within error, to the geodetic estimate of 9.3 ± 0.2 mm/a across this segment of the ECSZ [*Bennett et al.*, 2003]. Finally, taking into account the errors associated with each geologic slip rate estimate, the distribution of dextral shear across the ECSZ was concentrated along the northern Death Valley fault (~45%), with somewhat lesser slip along the Hunter Mountain fault (~35%). The remaining 20% of slip appears to be distributed equally along the two faults that bound the eastern California shear zone, the southern Owens Valley and Stateline faults.

8. Conclusions

[53] New geologic mapping, zircon and apatite (U-Th)/He ages, and ^{10}Be TCN alluvial fan surface abandonment ages along the eastern Inyo fault zone yield insight into the development of the Inyo Mountains as a major fault block within the ECSZ and western margin of the Basin and Range Province. We suggest that late Cretaceous/early Tertiary moderate to rapid exhumation of the range was related to Laramide deformation along the eastern margin of the present-day Sierra Nevada. Two episodes of normal slip along the EIFZ, initiation of slip at ~15.6 Ma and renewed slip at ~2.8 Ma, exhumed the Inyo Mountains in its footwall. The first episode of normal slip did not last longer than ~1.5 Ma, whereas the second episode continues today. The Inyo Mountains block was exhumed at an average,

Table 4. Pliocene to Holocene Dextral Slip Rates Along Major Strike-Slip Faults in the Eastern California Shear Zone as Well as a Calculated Slip Rate Sum Across the Zone[a]

Fault	Slip Rate (mm/a)[b]	Slip Rate (mm/a)[c]	Duration of Slip	Reference
State Line fault	1.0 ± 0.2	1.0 ± 0.2	present-day	*Wernicke et al.* [2004], *Hill and Blewitt* [2006]
Northern Death Valley fault	4.2 +1.9/−1.1 to 4.7 +0.9/−0.6	4.5 +1.6/−1.4	late Pleistocene	*Frankel et al.* [2007]
Hunter Mountain fault	3.3 ± 1.0	3.2 ± 1.0	late Pliocene	this work
Southern Owens Valley fault	1.0 ± 0.4	0.9 ± 0.4	Holocene	*Bacon and Pezzopane* [2007]
Slip rate sum 9.3 +2.2/−1.4 to 9.8 +1.4/−1.0				

[a]Slip rate data from this work and published estimates. Slip rates calculated at the latitude of ∼36.5°.
[b]Slip rate calculated parallel to strike of fault.
[c]Slip rate calculated parallel to Pacific-North America plate motion.

long-term dip slip rate of 0.5–1.2 mm/a. The initiation of slip at ∼15.6 Ma along the EIFZ is similar in age to initiation of normal slip along major range bounding normal faults within the western margin of the Basin and Range Province. This set of en echelon normal fault blocks may have defined the western boundary of the Basin and Range Province east of the present-day Sierra Nevada during the Miocene. The second episode of normal slip signals the onset of dextral slip along the Hunter Mountain fault, one of four major dextral faults that accommodate dextral shear across the ECSZ. Summing dextral slip rates on the Owens Valley, Hunter Mountain, northern Death Valley, and Stateline faults at the latitude of ∼36.5° yields long-term geologic slip rates of 7.9–11.2 mm/a, the same as geodetic rates across this part of the ECSZ. Taking into account errors associated with each geologic slip rate estimate, the northern Death Valley fault accommodated most of the dextral slip rate across the ECSZ.

[54] **Acknowledgments.** Tom Budlong's knowledge of the early to middle 20th century miners' trails in the Inyo Mountains was instrumental to successfully collecting (U-Th)/He samples across the mountains. Thanks to Tom Budlong, Jeff Schroeder, Kit Tincher, and Kelly Wooten for their assistance in collecting these samples. Jeff Schroeder also helped with differential GPS surveying. John Casteel, Yeong Bae Seong, Scott Heiztler, John Oswald, and Sam Clemens lent a hand with collection of the TCN samples. Stephanie Brichau managed the (U-Th)/He laboratory at the University of Kansas and trained one us (J.L.) in the art of picking apatites for analyses. Kurt Frankel, an anonymous reviewer, and Associate Editor Todd Ehlers provided thoughtful comments that improved this manuscript. This research was supported by National Science Foundation grants EAR-0207365 and EAR-0125782 awarded to J.L., EAR-0414817 awarded to D.S., and EAR-0207245 awarded to L.O.

References

Applegate, J. D. R., J. D. Walker, and K. V. Hodges (1992), Late Cretaceous extensional unroofing in the Funeral Mountains metamorphic core complex, California, *Geology*, *20*, 519–522.

Atwater, T., and J. Stock (1998), Pacific-North America plate tectonics of the Neogene southwestern United States: An update, *Int. Geol. Rev.*, *40*, 375–402.

Bacon, S. N., and S. K. Pezzopane (2007), A 25000-year record of earthquakes on the Owens Valley fault near Lone Pine, California: Implications for recurrence intervals, slip rates, and segmentation models, *Geol. Soc. Am. Bull.*, *119*, 823–847, doi:10.1130/B25879.1.

Bacon, S. N., A. S. Jayko, and J. P. McGeehin (2005), Holocene and latest Pleistocene oblique dextral faulting on the southern Inyo Mountains fault, Owens Lake Basin, California, *Bull. Seismol. Soc. Am.*, *95*, 2472–2485, doi:10.1785/0120040228.

Bartley, J. M., A. F. Glazner, D. S. Coleman, A. Kylander-Clark, R. Mapes, and A. M. Friedrich (2007), Large Laramide dextral offset across Owens Valley, California, and its possible relation to tectonic unroofing of the southern Sierra Nevada, in *Exhumation Associated With Continental Strike-Slip Fault Systems*, edited by A. B. Till et al., pp. 129–148, Geol. Soc. of Am., Boulder, Colo.

Bateman, P. C. (1992), Plutonism in the central part of the Sierra Nevada Batholith, California, *U.S. Geol. Surv. Prof. Pap. 1483*, U.S. Geol. Surv., Reston, Va.

Bateman, P. C., L. D. Clark, N. K. Huber, J. G. Moore, and C. D. Rinehart (1963), The Sierra Nevada batholith: A synthesis of recent work across the central part, *U.S. Geol. Surv. Prof. Pap. 0414-D*, U.S. Geol. Surv., Reston, Va.

Bennett, R. A., B. P. Wernicke, N. A. Niemi, A. M. Friedrich, and J. L. Davis (2003), Contemporary strain rates in the northern Basin and Range Province from GPS data, *Tectonics*, *22*(2), 1008, doi:10.1029/2001TC001355.

Blakely, R. J., and D. A. Ponce (2001), Map showing depth to pre-Cenozoic basement in the Death Valley ground-water model area, Nevada and California, *U.S. Geol. Surv. Misc. Field Stud. Map MF-2361–3*, scale 1:250000, U.S. Geol. Surv., Reston, Va.

Burchfiel, B. C., and J. H. Stewart (1966), "Pull-apart" origin of the central segment of Death Valley, California, *Geol. Soc. Am. Bull.*, *77*, 439–442, doi:10.1130/0016-7606(1966)77[439:POOTCS]2.0.CO;2.

Burchfiel, B. C., K. V. Hodges, and L. H. Royden (1987), Geology of Panamint Valley-Saline Valley pull-apart system, California: Palinspastic evidence for low-angle geometry of a Neogene range-bounding fault, *J. Geophys. Res.*, *92*, 10,422–10,426, doi:10.1029/JB092iB10p10422.

Casteel, J. C. (2005), Late Miocene to Holocene faulting along the southwestern Inyo Mountains fault zone, eastern California, M.S. thesis, 72 pp., Cent. Wash. Univ., Ellensburg, Wash.

Clark, M. K., G. Maheo, J. Saleeby, and K. A. Farley (2005), The non-equilibrium landscape of the southern Sierra Nevada, California, *GSA Today*, *15*, 4–10, doi:10.1130/1052-5173(2005)015[4:TNLOTS]2.0.CO;2.

Conrad, J. E. (1993), Late Cenozoic tectonics of the southern Inyo Mountains, eastern California, M.S. thesis, 84 pp., San Jose State Univ., San Jose, Calif.

Dickinson, W. R. (2002), The basin and range province as a composite extensional domain, *Int. Geol. Rev.*, *44*, 1–38, doi:10.2747/0020-6814.44.1.1.

Dilles, J. H., and P. B. Gans (1995), The chronology of Cenozoic volcanism and deformation in the Yerington Area, western Basin and Range and Walker-Lane, *Geol. Soc. Am. Bull.*, *107*, 474–486, doi:10.1130/0016-7606(1995)107<0474:TCOCVA>2.3.CO;2.

Dixon, T. H., S. Robaudo, J. Lee, and M. C. Reheis (1995), Constraints on present-day Basin and Range deformation from space geodesy, *Tectonics*, *14*, 755–772, doi:10.1029/95TC00931.

Dixon, T. H., M. M. Miller, F. Farina, H. Wang, and D. Johnson (2000), Present-day motion of the Sierra Nevada block and some tectonic implications for the Basin and Range province, North American Cordillera, *Tectonics*, *19*, 1–24.

Dokka, R. K., and C. J. Travis (1990), Late Cenozoic strike-slip faulting in the Mojave Desert, California, *Tectonics*, *9*, 311–340, doi:10.1029/TC009i002p00311.

Ducea, M. N., and J. B. Saleeby (1996), Buoyancy sources for a large, unrooted mountain range, the Sierra Nevada, California: Evidence from xenolith thermobarometry, *J. Geophys. Res.*, *101*, 8229–8244, doi:10.1029/95JB03452.

Dumitru, T. A. (1990), Subnormal Cenozoic geothermal gradients in the extinct Sierra Nevada magmatic arc: Consequences of Laramide and post-Laramide shallow-angle subduction, *J. Geophys. Res.*, *95*, 4925–4941, doi:10.1029/JB095iB04p04925.

Dunne, G. C. (1971), Petrology of the Pat Keyes pluton and its relation to the Sierra Nevada batholith, *Geol. Soc. Am. Abstr. Programs*, *8*, 113–114.

Dunne, G. C., and J. D. Walker (2004), Structure and evolution of the east Sierran thrust system, east central California, *Tectonics*, *23*, TC4012, doi:10.1029/2002TC001478.

Dunne, G. C., T. P. Garvey, M. Oborne, D. Schneidereit, A. E. Fritsche, and J. D. Walker (1998), Geology of the Inyo Mountains volcanic complex: Implications for Jurassic paleogeography of the Sierran magmatic arc in eastern California, *Geol. Soc. Am. Bull.*, *110*, 1376–1397, doi:10.1130/0016-7606(1998)110<1376:GOTIMV>2.3.CO;2.

Ehlers, T. A. (2005), Crustal thermal processes and the interpretation of thermochronometric data, in *Low-Temperature Thermochronology: Techniques, Interpretations, and Applications*, *Rev. Mineral. Geochem.*, vol. 58, edited by R. W. Reiners and T. A. Ehlers, pp. 315–350, Mineral. Soc. of Am., Chantilly, Va.

Elliot, G. S., C. T. Wrucke, and S. S. Nedell (1984), K-Ar ages of late Cenozoic volcanic rocks from the northern Death Valley region, *Isochron West*, *40*, 3–7.

Farley, K. A. (2000), Helium diffusion from apatite: General behavior as illustrated by Durango fluorapatite, *J. Geophys. Res.*, *105*, 2903–2914, doi:10.1029/1999JB900348.

Farmer, G. L., A. F. Glazner, and C. R. Manley (2002), Did lithospheric delamination trigger late Cenozoic potassic volcanism in the southern Sierra Nevada, California?, *Geol. Soc. Am. Bull.*, *114*, 754–768, doi:10.1130/0016-7606(2002)114<0754:DLDTLC>2.0.CO;2.

Fitzgerald, P. G. (1992), The Transantarctic Mountains of southern Victoria Land: The application of apatite fission track analysis to a rift shoulder uplift, *Tectonics*, *11*, 634–662, doi:10.1029/91TC02495.

Flesch, L. M., W. E. Holt, A. J. Haines, and B. Shen-Tu (2000), Dynamics of the Pacific-North American plate boundary in the western United States, *Science*, *287*, 834–836, doi:10.1126/science.287.5454.834.

Foster, D. A., and A. J. W. Gleadow (1996), Structural framework and denudation history of the flanks of the Kenya and Anza Rifts, east Africa, *Tectonics*, *15*, 258–271, doi:10.1029/95TC02744.

Frankel, K. L., et al. (2007), Cosmogenic 10Be and 36Cl geochronology of offset alluvial fans along the northern Death Valley fault zone: Implications for transient strain in the eastern California shear zone, *J. Geophys. Res.*, *112*, B06407, doi:10.1029/2006JB004350.

Gan, W., J. L. Svarc, J. C. Savage, and W. H. Prescott (2000), Strain accumulation across the eastern California shear zone at latitude 36°30′N, *J. Geophys. Res.*, *105*, 16,229–16,236, doi:10.1029/2000JB900105.

Glazner, A. F., J. Lee, J. M. Bartley, D. S. Coleman, A. Kylander-Clark, D. C. Greene, and K. Le (2005), Large dextral offset across Owens Valley, California from 148 Ma to 1872 A.D., in *Western Great Basin Geology*, *Pac. Sect. Soc. Sediment. Geol. Ser.*, vol. 99, edited by C. Stevens and J. Cooper, pp. 1–35, Soc. of Sediment. Geol., Tulsa, Okla.

Guest, B., N. A. Niemi, and B. P. Wernicke (2007), Stateline fault system: A new component of the Miocene-Quaternary eastern California shear zone, *Geol. Soc. Am. Bull.*, *119*, 1337–1346.

Hammond, W. C., and W. Thatcher (2004), Contemporary tectonic deformation of the Basin and Range province, western United States: 10 years of observation with the Global Positioning System, *J. Geophys. Res.*, *109*, B08403, doi:10.1029/2003JB002746.

Hanks, T. C., R. C. Bucknam, K. R. Lajoie, and R. E. Wallace (1984), Modification of wave-cut and fault controlled landforms, *J. Geophys. Res.*, *89*, 5771–5790, doi:10.1029/JB089iB07p05771.

Henry, C. D., and M. E. Perkins (2001), Sierra Nevada—Basin and Range transition near Reno, Nevada: Two-stage development at 12 and 3 Ma, *Geology*, *29*, 719–722, doi:10.1130/0091-7613(2001)029<0719:SNBART>2.0.CO;2.

Hill, E. M., and G. Blewitt (2006), Testing for fault activity at Yucca Mountain, Nevada, using independent GPS results from the BARGEN network, *Geophys. Res. Lett.*, *33*, L14302, doi:10.1029/2006GL026140.

House, M. A., B. P. Wernicke, K. A. Farley, and T. A. Dumitru (1997), Cenozoic thermal evolution of the central Sierra Nevada, California, from (U-Th)/He thermochronometry, *Earth Planet. Sci. Lett.*, *151*, 167–179, doi:10.1016/S0012-821X (97)81846-8.

House, M. A., K. A. Farley, and B. P. Kohn (1999), An empirical test of helium diffusion in apatite: Borehole data from the Otway Basin, Australia, *Earth Planet. Sci. Lett.*, *170*, 463–474, doi:10.1016/S0012-821X (99)00120-X.

House, M. A., B. P. Wernicke, and K. A. Farley (2001), Paleo-geomorphology of the Sierra Nevada, California, from (U-Th)/He ages in apatite, *Am. J. Sci.*, *301*, 77–102, doi:10.2475/ajs.301.2.77.

Jones, C. H., G. L. Farmer, and J. Unruh (2004), Tectonics of Pliocene removal of lithosphere of the Sierra Nevada, California, *Geol. Soc. Am. Bull.*, *116*, 1408–1422, doi:10.1130/B25397.1.

Kistler, R. W. (1993), Mesozoic paleogeography of the western United States—II, in *Mesozoic Intrabatholithic Faulting*, edited by G. C. Dunne and K. A. McDougall, pp. 247–261, Soc. of Econ. Paleontol. and Mineral., Sierra Nevada, Calif.

Kylander-Clark, A., D. S. Coleman, A. F. Glazner, and J. M. Bartley (2005), Evidence for 65 km of dextral slip across Owens Valley, California, since 83 Ma, *Geol. Soc. Am. Bull.*, *117*, 962–968, doi:10.1130/B25624.1.

Larsen, N. W. (1979), Chronology of late Cenozoic basaltic volcanism: The tectonic implications along a segment of the Sierra Nevada and Basin and Range Province boundary, Ph.D. thesis, 95 pp., Brigham Young Univ., Provo, Utah.

Le, K., J. Lee, L. A. Owen, and R. Finkel (2007), Late Quaternary slip rates along the Sierra Nevada frontal fault zone, California: Slip partitioning across the western margin of the eastern California shear zone-Basin and Range Province, *Geol. Soc. Am. Bull.*, *119*, 240–256, doi:10.1130/B25960.1.

Lee, J., C. M. Rubin, and A. Calvert (2001), Quaternary faulting history along the Deep Springs Fault, California, *Geol. Soc. Am. Bull.*, *113*, 855–869, doi:10.1130/0016-7606(2001)113<0855:QFHATD>2.0.CO;2.

Loomis, D. P., and D. W. Burbank (1988), The stratigraphic evolution of the El Paso Basin, southern California: Implications for the Miocene development of the Garlock Fault and uplift of the Sierra Nevada, *Geol. Soc. Am. Bull.*, *100*, 12–28, doi:10.1130/0016-7606(1988)100<0012:TSEOTE>2.3.CO;2.

Manley, C. R., A. F. Glazner, and G. L. Farmer (2000), Timing of volcanism in the Sierra Nevada of California: Evidence for Pliocene delamination of the batholithic root?, *Geology*, *28*, 811–814, doi:10.1130/0091-7613(2000)28<811:TOVITS>2.0.CO;2.

Marrett, R., and R. W. Allmendinger (1990), Kinematic analysis of fault-slip data, *J. Struct. Geol.*, *12*, 973–986, doi:10.1016/0191-8141(90)90093-E.

Miller, M. B., and T. L. Pavlis (2005), The Black Mountains turtlebacks: Rosetta stones of Death Valley tectonics, *Earth Sci. Rev.*, *73*, 115–138, doi:10.1016/j.earscirev.2005.04.007.

Miller, M. G. (2003), Basement-involved thrust faulting in a thin-skinned fold-and-thrust belt, Death Valley, California, USA, *Geology*, *31*, 31–34.

Miller, M. G., and R. M. Friedman (1999), Early Tertiary magmatism and probable Mesozoic fabrics in the Black Mountains, Death Valley, California, *Geology*, *27*, 19–22.

O'Malley, P. A. (1980), Quaternary geology and tectonics of the Waucoba Wash 15-minute quadrangle Saline Valley, Inyo County, California, M.S. thesis, 142 pp., Univ. of Nev., Reno, Reno, Nev.

Oskin, M., and A. Iriondo (2004), Large-magnitude transient strain accumulation on the Blackwater fault, eastern California shear zone, *Geology*, *32*, 313–316, doi:10.1130/G20223.1.

Oskin, M., L. Perg, D. Blumentritt, S. Mukhopadhyay, and A. Iriondo (2007), Slip rate of the Calico fault: Implications for geologic versus geodetic rate discrepancy in the eastern California shear zone, *J. Geophys. Res.*, *112*, F03S03, doi:10.1029/2006JF000563.

Oswald, J. A., and S. G. Wesnousky (2002), Neotectonics and Quaternary geology of the Hunter Mountain fault zone and Saline Valley region, southeastern California, *Geomorphology*, *42*, 255–278, doi:10.1016/S0169-555X (01)00089-7.

Pakiser, L. C., M. F. Kane, and W. H. Jackson (1964), Structural geology and volcanism of Owens Valley region, California: A geophysical study, *U.S. Geol. Surv. Prof. Pap. 0438*, 68 pp., Reston, Va.

Peltzer, G., F. Crampe, S. Hensley, and P. Rosen (2001), Transient strain accumulation and fault interaction in the eastern California shear zone, *Geology*, *29*, 975–978, doi:10.1130/0091-7613(2001)029<0975:TSAAFI>2.0.CO;2.

Reiners, P. W. (2005), Zircon (U-Th)/He thermochronometry, in *Low-Temperature Thermochronology: Techniques, Interpretations, and Applications*, *Rev. Mineral. Geochem.*, vol. 58, edited by R. W. Reiners and T. A. Ehlers, pp. 151–179, Mineral. Soc. of Am., Chantilly, Va.

Reiners, P. W., R. Brady, K. A. Farley, J. E. Fryxell, B. P. Wernicke, and D. Lux (2000), Helium and argon thermochronometry of the Gold Butte block, South Virgin Mountains, Nevada, *Earth Planet. Sci. Lett.*, *178*, 315–326, doi:10.1016/S0012-821X(00)00080-7.

Rockwell, T. K., S. Lindvall, M. Herzberg, D. Murbach, T. Dawson, and G. Berger (2000), Paleoseismology of the Johnson Valley, Kickapoo, and Homestead Valley faults: Clustering of earthquakes in the eastern California shear zone, *Bull. Seismol. Soc. Am.*, *90*, 1200–1236, doi:10.1785/0119990023.

Ross, D. C. (1965), Geology of the Independence Quadrangle, Inyo County, California, Series Geology of the Independence Quadrangle, Inyo County, California, *U.S. Geol. Surv. Bull. B1181-O*, U.S. Geol. Surv., Reston, Va.

Ross, D. C. (1967), Generalized geologic map of the Inyo Mountains region, California, *U.S. Geol. Surv. Misc. Geol. Invest. Map*, *I-0506*, scale 1:125000, U.S. Geol. Surv., Reston, Va.

Ross, D. C. (1969), Descriptive petrography of three large granitic bodies in the Inyo Mountains, California, *U.S. Geol. Surv. Prof. Pap. 601*, 47 pp., U.S. Geol. Surv., Reston, Va.

Ross, D. C. (1970), Pegmatitic trachyandesite plugs and associated volcanic rocks in the Saline Range-Inyo mountains region, California, *U.S. Geol. Surv. Prof. Pap. 0614-D*, U.S. Geol. Surv., Reston, Va.

Sonder, L. J., and C. H. Jones (1999), Western United States extension: How the west was widened, *Annu. Rev. Earth Planet. Sci.*, *27*, 417–462, doi:10.1146/annurev.earth.27.1.417.

Sternlof, K. R. (1988), Structural style and kinematic history of the active Panamint-Saline extensional system, Inyo County, California, M.S. thesis, 40 pp., Mass. Inst. of Technol., Cambridge, Mass.

Stevens, C. H., W. G. Ernst, P. Stone, G. C. Dunne, D. C. Greene, J. D. Walker, B. J. Swanson, and B. J. Skinner (1997), Paleozoic and Mesozoic evolution of east-central California, *Int. Geol. Rev.*, *39*, 788–829.

Stock, G. M., R. S. Anderson, and R. C. Finkel (2004), Pace of landscape evolution in the Sierra Nevada, California, revealed by cosmogenic dating of cave sediments, *Geology*, *32*, 193–196, doi:10.1130/G20197.1.

Stockli, D. F. (2005), Application of low-temperature thermochronology to extensional tectonic settings, in *Low-Temperature Thermochronology: Techniques, Interpretations, and Applications*, *Rev. Mineral. Geochem.*, vol. 58, edited by R. W. Reiners and T. A. Ehlers, pp. 411–448, Mineral. Soc. of Am., Chantilly, Va.

Stockli, D. F., K. A. Farley, and T. A. Dumitru (2000), Calibration of the apatite (U-Th)/He thermochronometer on an exhumed fault block, White Mountains, *Calif. Geol.*, *28*, 983–986.

Stockli, D. F., B. E. Surpless, T. A. Dumitru, and K. A. Farley (2002), Thermochronological constraints on the timing and magnitude of Miocene and Pliocene extension in the central Wassuk Range, western

Nevada, *Tectonics*, *21*(4), 1028, doi:10.1029/2001TC001295.

Stockli, D. F., T. A. Dumitru, M. O. McWilliams, and K. A. Farley (2003), Cenozoic tectonic evolution of the White Mountains, California and Nevada, *Geol. Soc. Am. Bull.*, *115*, 788–816, doi:10.1130/0016-7606(2003)115<0788:CTEOTW>2.0.CO;2.

Stone, P., G. C. Dunne, J. E. Conrad, B. J. Swanson, C. H. Stevens, and Z. C. Valin (2004), Geologic map of the Cerro Gordo Peak 7.5′ quadrangle, Inyo County, California, *U.S. Geol. Surv. Sci. Invest. Map 2851*, scale 1:24000, 17 pp., U.S. Geol. Surv., Reston, Va.

Surpless, B. E., D. F. Stockli, T. A. Dumitru, and E. L. Miller (2002), Two-phase westward encroachment of Basin and Range extension into the northern Sierra Nevada, *Tectonics*, *21*(1), 1002, doi:10.1029/2000TC001257.

Sylvester, A. G., G. Oertel, C. A. Nelson, and J. M. Christie (1978), Papoose Flat Pluton: A granitic blister in the Inyo Mountains, California, *Geol. Soc. Am. Bull.*, *89*, 1205–1219, doi:10.1130/0016-7606(1978)89<1205:PFPAGB>2.0.CO;2.

Tagami, T., K. A. Farley, and D. F. Stockli (2003), (U-Th)/He geochronology of single zircon grains of known Tertiary eruption age, *Earth Planet. Sci. Lett.*, *207*, 57–67, doi:10.1016/S0012-821X (02)01144-5.

Unruh, J. (1991), The uplift of the Sierra Nevada and implications for late Cenozoic epeirogeny in the western Cordillera, *Geol. Soc. Am. Bull.*, *103*, 1395–1404, doi:10.1130/0016-7606(1991)103<1395:TUOTSN>2.3.CO;2.

Wakabayashi, J., and T. L. Sawyer (2001), Stream incision, tectonics, uplift, and evolution of topography of the Sierra Nevada, California, *J. Geol.*, *109*, 539–562, doi:10.1086/321962.

Wells, M. L., and T. D. Hoisch (2008), The role of mantle delamination in widespread Late Cretaceous extension and magmatism in the Cordilleran Orogen, western United States, *Geol. Soc. Am. Bull.*, *120*, 515–530, doi:10.1130/B26006.1.

Wernicke, B. P., J. L. Davis, R. A. Bennett, J. E. Normandeau, A. M. Friedrich, and N. A. Niemi (2004), Tectonic implications of a dense continuous GPS velocity field at Yucca Mountain, Nevada, *J. Geophys. Res.*, *109*, B12404, doi:10.1029/2003JB002832.

Wolf, R. A., K. A. Farley, and L. T. Silver (1996), Helium diffusion and low temperature thermochronometry of apatite, *Geochim. Cosmochim. Acta*, *60*, 4231–4240, doi:10.1016/S0016-7037(96)00192-5.

Wolf, R. A., K. A. Farley, and D. M. Kass (1998), Modeling of the temperature sensitivity of the apatite (U-Th)/He thermochronometer, *Chem. Geol.*, *148*, 105–114, doi:10.1016/S0009-2541(98)00024-2.

Wolfe, M. R., D. F. Stockli, D. L. Shuster, J. D. Walker, and G. L. Macpherson (2007), Assessment of the rutile (U-Th)/He thermochronometry on the KTB drill hole, Germany, *Eos Trans. AGU*, *88*(52), Fall Meet. Suppl., Abstract V23C–1549.

Wood, J., and J. Saleeby (1997), Late Cretaceous-Paleocene extensional collapse and disaggregation of the southernmost Sierra Nevada batholith, *Int. Geol. Rev.*, *39*, 973–1009.

Zandt, G., H. Gilbert, T. J. Owens, M. Ducea, J. Saleeby, and C. H. Jones (2004), Active foundering of a continental arc root beneath the southern Sierra Nevada in California, *Nature*, *431*, 41–46, doi:10.1038/nature02847.

Zeitler, P. K., A. L. Herczeg, I. McDougall, and M. Honda (1987), U-Th-He dating of apatite: A potential thermochronometer, *Geochim. Cosmochim. Acta*, *51*, 2865–2868, doi:10.1016/0016-7037(87)90164-5.

R. C. Finkel, Center for Accelerator Mass Spectrometry, Lawrence Livermore National Laboratory, Livermore, CA 94550, USA.

R. Kislitsyn and D. F. Stockli, Department of Geology, University of Kansas, 1475 Jayhawk Boulevard, Room 120, Lawrence, KS 66045-7613, USA.

J. Lee, Department of Geological Sciences, Central Washington University, 400 East University Way, Ellensburg, WA 98926, USA. (jeff@geology.cwu.edu)

L. A. Owen, Department of Geology, University of Cincinnati, P.O. Box 0013, Cincinnati, OH 45221-0013, USA.